Characterization of the chemical bonding at the interfaces of SiO_2-related materials using microscopic infrared spectroscopy and attenuated total reflection

A Thesis for the Degree

of

Doctor of Engineering

Submitted to

School of Science and Technology

Kwansei-Gakuin University

By

Hirofumi Seki

in January 2017.

CONTENTS

General introduction 1

Motivation and background to the research 2
Previous research and adaptation of FT-IR analysis for semiconductor materials 4
Novelty and originality of this research 6
Outline of this study 7
References 9

Chapter.1: Characterization of Ashing Damage in Depth Direction in Low-k Dielectric Films by Microscopic IR Method 19

Abstract 20
Introduction 21
Experimental detail 22
Result and discussion 23
Conclusion 26
References 27

Chapter.2: Characterization of process-induced damage in Cu/low-k interconnect structure by microscopic infrared spectroscopy with polarized infrared light 36

Abstract 37
Introduction 38
Experimental detail 40
Result and discussion 42
Conclusion 46
References 48

Chapter.3: Characterization of Inhomogeneity in SiO_2 Films on 4H-SiC Epitaxial Substrate by a Combination of Fourier Transform Infrared and Cathodoluminescence Spectroscopy 63

Abstract 64
Introduction 65
Experimental detail 68
Result and discussion 70

Conclusion 75
References 76

Chapter.4: Characterization of Thermal Oxides on 4H-SiC Epitaxial Substrates Using Fourier-Transform Infrared Spectroscopy 86

Abstract 87
Introduction 88
Experimental detail 90
Result and discussion 92
Conclusion 98
References 100

List of publications 112

Acknowledgement 115

Abbreviations

AES: Auger Electron Spectroscopy

AFM: Atomic Force Microscopy

ATR: Attenuated Total Reflection

ASTM: American Society for Testing and Materials

CCD: Charge Coupled Device

CL: Cathodoluminescence

CM: Channel Mobility

CMP: Chemical Mechanical Polishing

CVD: Chemical Vapor Deposition

D_{it}: Interface trap density

EDX: Energy Dispersive X-ray analysis

EELS: Electron Energy-Loss Spectroscopy

EPMA: Electron Probe Microanalyzer

ESR: Electron Spin Resonance

HFS: Hydrogen Forward Scattering

FT-IR: Fourier Transform Infrared Spectroscopy

GSP: Gradient Shaving Preparation

ICP-MS: Inductively Coupled Plasma Mass Spectrometer

ISSG: In-Situ Steam Generation

MOSFET: Metal-Oxide Semiconductor Field-Effect Transistor

MSQ: Methyl Silsequioxane

NBOHC: Non-Bridging Oxidation Hole Center

NMR: Nuclear Magnetic Resonance analysis

OVC: Oxygen Vacancy Center

PALS: Positron Annihilation Lifetime Spectroscopy

POA: Post Oxidation Annealing

PL: Photoluminescence

Q_{eff}: Effective fixed charge density

Raman: Raman scattering spectroscopy

RBS: Rutherford Back Scattering Spectrometry

RTO: Rapid Thermal Oxidation

SCM: Scanning Capacitance Microscope

SEM: Scanning Electron Microscopy

SEMI: Semiconductor Equipment and Materials International

SIMS: Secondary Ion Mass Spectroscopy

SPP: Surface Phonon Polariton

SR: Spreading Resistance

SSRM: Scanning Spreading Resistance Microscopy

STM: Scanning Tunneling Microscopy

ULSI: Ultra Large Scale Integration

TEM: Transmission Electron Microscopy

TO: Transverse Optic

TOF-SIMS: Time-of-Flight Secondary Ion Mass Spectrometry

XPS: X-ray Photoelectron Spectroscopy

XRD: X-ray Diffractometry

XRF: X-ray Fluorescence analysis

XRR: X-ray Reflectometry

General Introduction

Motivation and background to this research

Semiconductors, as exemplified by ultra large scale integration (ULSI) devices, currently feature high-density integration as a result of the miniaturization of their design. They have conformed to Moore's Law in that the number of transistors in a dense integrated circuit has doubled approximately every two years.[1)] The size of the gate electrodes of semiconductors was originally on the micrometer level, but has gradually become smaller and now is typically less than 100 nm. Manufacturing based on a design rule of the several nm level has been the subject of considerable study such that it is gradually being commercialized. To miniaturize semiconductor devices, different materials, each offering their own unique advantages, have been adopted. For example, wiring was originally fabricated using aluminum, while copper is commonly used now. Meanwhile, the interlayer insulator material between the wiring layers has changed from silicon dioxide (SiO_2) to a low dielectric value material (Low-k material) that incorporates organic components. Gate insulator films, which were originally silicon dioxide (SiO_2), are now formed using high-k films such as hafnium oxide or hafnium silicate.[2, 3)]
As manufacturing design rules approach the nm level, the miniaturization of transistors is approaching its limit. In recent years, some aggressive research addressing the improvement of devices has considered 3-dimensional integration or has introduced new materials. Multi-functionality has been achieved by adding sensors, detectors, and so on. [2)] On the other hand, in the area of semiconductor substrates, the use of Si has been proposed, but Ge substrates and next-generation materials of the III-V groups are also being studied. Silicon carbide (SiC) substrates are already being used in power devices instead of a Si substrate. The use of a gallium nitride (GaN) substrate has also been the subject of various studies.[4-6)]

Semiconductor devices, such as those used in smartphones, are indispensable to our daily lives. In addition, automotive applications of semiconductors, such as for sensors, have expanded, with quality and reliability demands becoming more severe. Given that semiconductor devices have multilayer structures incorporating different materials, the manufacturing process has become extremely complicated, and the processing technology has become clearly divided into very wide segments. In addition, as materials become thinner, the surface and interface properties of thin films are important in that they have a critical effect on the device performance. For this reason, it is extremely important to have a method in place for evaluating ultra-thin films or very small regions, and to identify the physical

parameters that affect the electrical characteristics while developing the manufacturing process. Therefore, analytical techniques are indispensable to semiconductor process development in that they provide a means of searching for and evaluating such physical parameters.

Analytical techniques for semiconductors are summarized in Table 1-1. The main techniques for analyzing semiconductors are transmission electron microscope (TEM) observations to confirm the actual nm-level device structure, secondary ion mass spectrometer (SIMS) analysis to confirm the depth profile of impurities that affect the electrical property, and inductively coupled plasma mass spectrometer (ICP-MS) analysis to quantify the trace impurities. These techniques are widely used and are well-established analytical techniques. Meanwhile, in spectroscopic analysis methods such as Fourier transform infrared (FT-IR) and Raman spectroscopy, characteristic information such as the chemical bonding state information is obtained by spectroscopic methods, providing information which cannot be obtained by other means. However, there are several problems related to the analysis of the ultra-thin films found in semiconductor devices. One is that the analysis is very difficult because spectral data are obtained by the measurements and spectral analysis requires considerable experience and knowledge. Fig. 1-1 shows the spatial resolution and the amount of chemical structure information produced by the analytical techniques applied to semiconductors. The unit size of semiconductor devices is nowadays approaching the nm scale due to the miniaturization described above, consequently requiring the ability to conduct analyses of a very small area. As can be seen from the figure, spectroscopic methods such as FT-IR and Raman spectroscopy provide rich information about the chemical structure, but the spatial resolution is in the order of microns, making it difficult to directly apply these to the analysis of semiconductor devices. Fig. 1-2 compares the depth resolution for each analysis method. FT-IR has a depth resolution of the submicron to micron order, whereas other surface analysis methods have a resolution on the order of nanometers, making them unsuitable for application to the analysis of ultra-thin films with a smaller thickness. However, FT-IR has been used as an effective means of analyzing SiO_2 films for a long time, and is well covered by the literature.[7-22] It is expected that it will be possible to obtain useful information by adapting FT-IR to the evaluation of semiconductor devices.

Therefore, this study sets out to establish a tool for evaluating the process development of a semiconductor device by using FT-IR analysis. The author considered analytical methods for evaluating the depth direction and interfaces of thin films, based on FT-IR. The author

overcame the problems of low spatial resolution and low depth resolution that characterize FT-IR analysis by improving the pretreatment and measurement methods while attempting to establish a method for evaluating semiconductor materials, especially the manufacturing process development of SiO_2 materials for which FT-IR has already successfully produced results. In particular, the author examined the methods used to evaluate the depth direction and interfaces of SiO_2 materials (especially low-k films and SiO_2 films formed on a SiC substrate) and compared the physical parameters obtained by these methods with the electrical properties. Finally, the author evaluated the effectiveness of each of the methods.

Previous research and adaptation of FT-IR analysis to semiconductor materials

FT-IR analysis of semiconductor materials

FT-IR is also widely utilized for inorganic materials such as semiconductors.[23)] For example, it is generally used for quantitative analyses of oxygen, carbon, and nitrogen in silicon and for determining the amounts of dopants (boron, phosphate, gallium, aluminum, etc.) at low temperatures (around 10 K). The technique is covered by international standards such as the SEMI International Standards and the ASTM standards.[24)] FT-IR is used to detecting the constituent gases in emissions and the gas concentrations in manufacturing chambers.[25)] FT-IR is often applied to the quantitative analysis of functional groups (the N-H and Si-H groups in silicon nitride film and the Si-H groups in amorphous silicon) in the areas of semiconductors and solar cells.[26-29)] It is useful for characterizing the photo reaction of resists and the degradation of organic materials such as resins or films.

Compared to other analytical techniques, FT-IR has some unique features in that it can be used to detect hydrogen-related bonds such as Si-H and C-H groups and moisture-related OH and metal-OH bonds. It provides a comparatively simple means of investigating the chemical bonding structure of a material.

Depth analysis of thin film by FT-IR method

The conventional methods of analyzing the depth direction of organic thin films are shown in Fig. 1-3. Evaluation-based methods include those in which cross-sectional processing is carried out and in which measurement is performed from the sectional direction shown in Fig. 1-3(a), while the FT-IR measurement is repeated while slowly removing material by means of mechanical polishing or ion milling, as shown in Fig. 1-3(b), (c). An example of depth

analysis is shown in Fig. 1-4. The chemical bonding state in the depth direction was evaluated in the depth direction, with a sub-micron resolution, by repeating the attenuated total reflection (ATR) method and the mechanical polishing for the adhesive layer at the polyimide film/copper thin film interface. The depth profile spectra were obtained at each measuring point. It is assumed that the amounts of carboxylate salt and OH groups increased. Therefore, the hydroxylation of the ester groups occurred. A depth analysis can be carried by repeating the mechanical polishing and ATR measurements for a thin film. However, it is difficult to carry out a depth direction analysis for submicron organic thin films when using mechanical polishing. In addition, in the case of ion milling, the organic film is damaged. While it is possible to discuss the depth distribution of the elemental information, it is difficult to argue the original chemical bonding state due to the deterioration of the organic film. Therefore, there is a need for a method of evaluating the chemical bonding state in submicron organic thin films. The author developed a new means of evaluating the state of chemical bonding in submicron organic thin films by introducing a new pretreatment method.

Use of FT-IR to evaluate damage in low-k films in device structure

A cross-sectional TEM photograph and a schematic view of the multilayer interconnection structure of a commercial LSI device are shown in Fig. 1-5. The semiconductor device has a structure in which different materials are stacked three-dimensionally. Low-k materials can be applied as dielectric interlayers to replace the SiO_2 dielectric layer.[5] Low-k materials basically consist of Si-O frameworks and Si-CH_3, Si-H terminal groups. Therefore, they incorporate many pores into the film to reduce the dielectric constant. However, low-k films have organic components and therefore tend to exhibit changes in their structure owing to plasma processes such as etching, ashing, and metal deposition. The structural changes in low-k films increase the dielectric constant and degrade the hygroscopic property. Therefore, it is necessary to investigate the process-induced damage to low-k films. Regarding there being no patterning of low-k films, there have been many studies using FT-IR.[30-33] However, as the thickness of a low-k film is of the submicron level, there have been no reports of evaluations of the chemical bond state of low-k films in the depth direction.

The TEM image shows how a low-k film is used as an interlayer insulating film, filling the spaces between the Cu wiring layers. In fact, it is important to evaluate the damage to the side walls and bottom of low-k films during trench formation processes. Although damage evaluations have been conducted by means of electron energy-loss spectroscopy

(TEM-EELS) or TEM observations after HF treatment, there have been very few reports of FT-IR evaluations of samples with such a trench structure.

Characterization of silicon dioxide by FT-IR analysis

SiO_2 films are remarkable and useful materials in the semiconductor industry. They exhibit good insulation properties and a uniform thickness. SiO_2 can dissolve in a HF acid solution, whereas Si substrates do not dissolve. A thin oxide film can thus be easily prepared by the oxidation of the Si substrate. Therefore, these properties enable the fabrication of metal oxide semiconductor field-effect transistors (MOSFET), which are a type of transistor used for amplifying or switching electronic signals. However, defects and impurities arise in a SiO_2 film, and it is difficult to control the properties of these films, as shown in Fig. 1-6. Many reports have focused on the characterization and improvement of SiO_2 films. [7-22] As the thickness and width of the film are made smaller, it is important to control the interfacial structures at the interface between the oxide and the substrate. Many researchers have investigated and improved these properties. In our group, a special wet pretreatment process was developed to form an incline on an ultra-thin SiO_2 film. It was found, using FT-IR, that the amount of Si-O peak shift at the SiO_2/Si interface is closely correlated to the leakage current, as shown in Fig.1-7.[9] In recent years, SiC substrates have been used for power devices.[6] However, there are several longstanding problems related to the high trap densities and the high fixed-charge density at the SiO_2/SiC interface; these high values can degrade the channel mobility of SiC MOSFETs. These problems are believed to be caused by poor interfacial properties. Therefore, the interfacial chemical bonding structure should be investigated by FT-IR analysis. However, although a few studies have used FT-IR analysis to investigate the application of SiO_2 films to SiC substrates, none have discussed the relationship between the chemical bonding structure and the electrical properties.

Novelty and originality of this study

In this study, the author developed a method for evaluating the ultra-thin films used in semiconductor devices.

The completely new depth direction analysis method can evaluate the chemical bonding state at depth intervals of several tens of nm. This can be applied not only to a low-k film but also to an ultra-thin film of sub-micron thickness, including the organic components that easily

degrade. In addition, the method enables depth direction analysis by applying not only FT-IR analysis but also other surface analysis methods to the inclined surface created by the newly introduced pretreatment method.

The author also developed a method for evaluating a trench structure sample with a Cu/low-k line and space structure. Previously, FT-IR had not been applied to non-patterned films, and therefore had not been used to evaluate a trench structure like that of a real device. By improving the sample structure and measurement method, the author was able to perform an evaluation of a trench structure by using FT-IR. This is a useful method that can be applied to the development of other semiconductor devices having a trench structure, such as dynamic random access memory (DRAM) and NAND flash memory.

The author characterized the chemical bonding structure at the SiO_2/SiC substrate interface by combining wet etching and the ATR method. Thus, a physical parameter that is related to the electrical properties was identified for the first time.

Outline of this study

This thesis is composed of four chapters and a preface. Each chapter is outlined below:

In the current chapter, the author describes the purpose of the research, previous research, the adaptation of FT-IR to semiconductor materials, and the novelty and originality of this research.

In Chapter 1, the author reports on the development of a useful pretreatment method (referred to as gradient shaving preparation (GSP)) to investigate the chemical bonding structure of sub-micron thickness thin films in the depth direction by using FT-IR measurements. The author investigates the chemical structure changes in the depth direction of low-k dielectric films, 250-nm thick, after several ashing processes, by using the microscopic FT-IR method, and characterizes the type and extent of the ashing damage in the low-k films. The author confirms that this pretreatment method is useful for characterizing the chemical bonding of thin organic film in the depth direction.

In Chapter 2, the author sets out to evaluate the process-induced damage for a Cu/low-k interconnect structure using polarized IR light for different widths of low-k spaces and Cu lines, and for different heights of Cu lines, on Si substrates. Although the width of both the Cu line and the low-k space is 70 nm, considerably smaller than the wavelength of IR light, FT-IR spectra of the low-k film were obtained for the Cu/low-k interconnect structure. A

suitable method was established for measuring the process-induced damage on the sidewalls of the low-k films that was not detected by TEM-EELS using microscopic IR polarized light.

In Chapter 3, the author presents the measured FT-IR and cathodoluminescence (CL) spectra of SiO_2 films grown on 4H-SiC substrates, confirming that the phonon observes the upper branch of the surface phonon polaritons (SPPs) in the SiO_2 films and that its frequency is sensitive to the oxide thickness. The relative intensity of the upper branch of SPPs normalized by that of the transverse optical phonon (TO) tended to increase as the channel mobility (CM) decreased. A comparison between the FT-IR and CL measurements shows that the relative intensity is correlated to the inhomogeneity in the SiO_2/SiC interface, and the CM of SiC devices.

In Chapter 4, the author presents the measured FT-IR spectra of thermal oxides with different electrical properties grown on 4H-SiC substrates and discusses the interfacial bonding structure and stresses in the depth direction as determined with repeated ATR measurements and wet etching. For the thinner thermal oxides (SiO_2 thicknesses of less than 3 nm), the peak frequency of the TO mode of the oxides on the 4H-SiC substrate is red-shifted as the oxide layer thickness decreases. The channel mobilities are correlated with the degree of the shift of the TO mode in samples with an oxide thickness of less than 3 nm. It appears that the compressive stress at the SiO_2/SiC interface generates silicon suboxide components and weakens the Si-O bonds. Therefore, the TO mode was red-shifted and the oxygen deficiency increased to relax the compressive stress in the oxide with < 3 nm thickness.

REFERENCES

[1]G.E. Moore,"Cramming more components onto integrated circuits," Electronics, 38, 114(1965).

[2]International Technology roadmap for Semiconductors (ITRS) 2008. www.itrs.net.

[3]J. Robertson, Solid-State Electron. 49, 283 (2005).

[4]V. Tilak, B. Green, V. Kaper, H. Kim, T. Prunty, J. Smart, et al., IEEE Electron Dev Lett. 22, 504 (2001).

[5]R.D. Goldblatt, B. Agarwala, M.B. Anand, E.P. Barth, G.A. Biery, Z.G. Chen, and S. Gohen, Proc. of IITC. 1, 261 (2000).

[6]J.A. Cooper, Jr, Phys. Stat. Sol. (a), 162(1), 305 (1997).

[7]C. Martinet and R.A.B. Devine, J. Appl. Phys. 77, 4343 (1995).

[8]K.T. Queeney, M.K. Weldon, J.P. Chang, Y.J. Chabal, A.B. Gurevich, J. Sapjeta, and R.L. Opila, J. Appl. Phys. 87, 1322 (2000).

[9]N. Nagai, K. Terada, Y. Muraji, H. Hashimoto, T. Maeda, Y. Maeda, E. Tahara, N. Tokai, and A. Hatta, J. Appl. Phys. 91, 4747 (2002).

[10]K. Kim, J. Song, D. Kwon, and G.S. Lee, Appl. Phys. Lett. 72, 1247–1249 (1998).

[11]I. Boyd and J. Wilson, Appl. Phys. Lett. 50, 320 (1987).

[12]M.L. Green, E.P. Gusev, R. Degraeve, and E.L. Garfunkel, J. Appl. Phys. 90, 2057 (2001).

[13]N. Hirashita, S. Tokitoh, and H. Uchida, Jpn. J. Appl. Phys. 32, 1787 (1993).

[14]J. Shiuh, Si-chen Lee, J. Appl. Phys. 77, 1805 (1995).

[15]T. Yamaguchi and N. Sakamoto, J. Appl. Phys. 83, 554 (1998).

[16]Y. Kim, M. Hwang, and H. Kim, J. Appl. Phys. 90, 3367 (2001).

[17]R. Nonogaki, S. Nakai, S. Yamada, and T. Wada, J. Vac. Sci. Technol. A. 16, 2827 (1998).

[18]P.G. Pai, S.S. Chao, Y. Takagi, and G. Locovsky, J. Vac. Sci. Technol. A. 4, 689 (1986).

[19]J.T. Fitch, G. Lucovsky, E. Kobeda, and E.A. Irene, J. Vac. Sci. Technol. B. 7, 153 (1989).

[20]G. Lucovsky, M.J. Manitini, J.K. Srivastava, and E.A. Irena, J. Vac. Sci. Technol. B5, 530

(1987).

[21]W.A. Pliskin and H.S. Lehman, J. Electrochem. Soc. 112, 1013 (1965).

[22]S. Miyazaki, H. Nishimura, M. Fukuda, L. Ley, and J. Ristein, Appl. Surf. Sci. 113/114. 585 (1997).

[23]M. Tasumi, Introduction to Experimental Infrared Spectroscopy, John Wiley & Sons, (2015).

[24]ASTM Designation F1188 – Test Method for Interstitial Atomic Oxygen Content of Silicon by Infrared Absorption, F1391 – Test Method for Substitutional Atomic Carbon Content by Infrared Absorption.

[25]R. Jaaniso and O.K. Ta, Semiconductor Gas Sensors, Woodhead Publishing Limited, (2013).

[26]W.A. Lanford and M. J. Rand, J. Appl. Phys. 49, 2473 (1978).

[27]G. Sasaki, M. Kondo, S. Fujita and A. Sasaki, Jpn. J. Appl. Phys. 21, 1394 (1982).

[28]G. Lucovsky, Solid State Commun. 29, 571 (1979).

[29]M.H. Brodsky et al., Phys. Rev. B16, 3556 (1977).

[30]A. Grill, J. Appl. Phys. 93, 1785 (2003).

[31]A. Grill and D.A. Neumayer, J. Appl. Phys. 94, 6697 (2003).

[32]B. Zhao and M. Brongo, Mater. Res. Soc. Symp. Proc. 565, 137 (1999).

[33]J.-N. Sun, D.W. Gidley, T.L. Dull, W.E. Frieze, A.F. Yee, E.T. Ryan, S. Lin, and J. Wetzel, J. Appl. Phys. 89, 5138 (2001).

Table. 1-1 Analysis methods for semiconductor devices.

Information	Analytical methods
Composition	SIMS, EPMA,TEM-EDX, EELS, AES, RBS, XRF, XPS
Chemical structure	FT-IR, XPS, NMR, Raman, TEM-EELS, AES
Morphology	TEM, SEM, AFM
Defect/crystallinity	TEM, CL, PL, Raman, XRD, ESR, FT-IR
Carrier concentration	SCM, SSRM, SR
Stress/strain	Raman, XRD, TEM
Roughness	AFM, STM, TEM, SEM, XRR
Voids	TEM, SEM, PALS
Thickness/density	Ellipsometry, XRR, RBS
Impurity profile	SIMS
Contamination	ICP-MS, TOF-SIMS

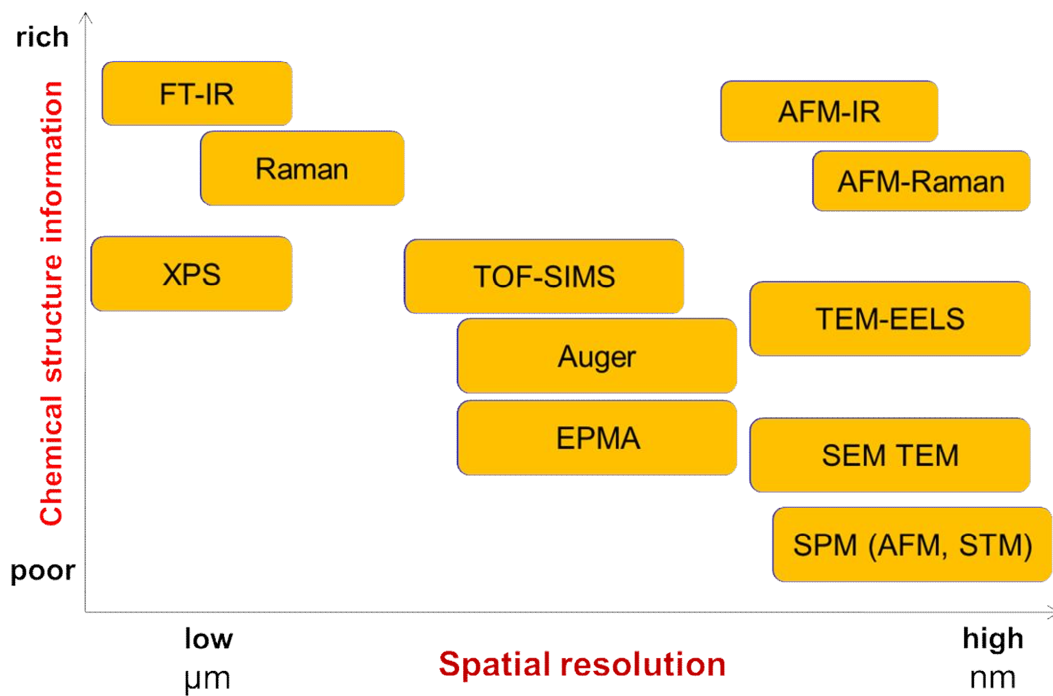

Fig. 1-1. Chemical structure information and spatial resolution for each analytical method

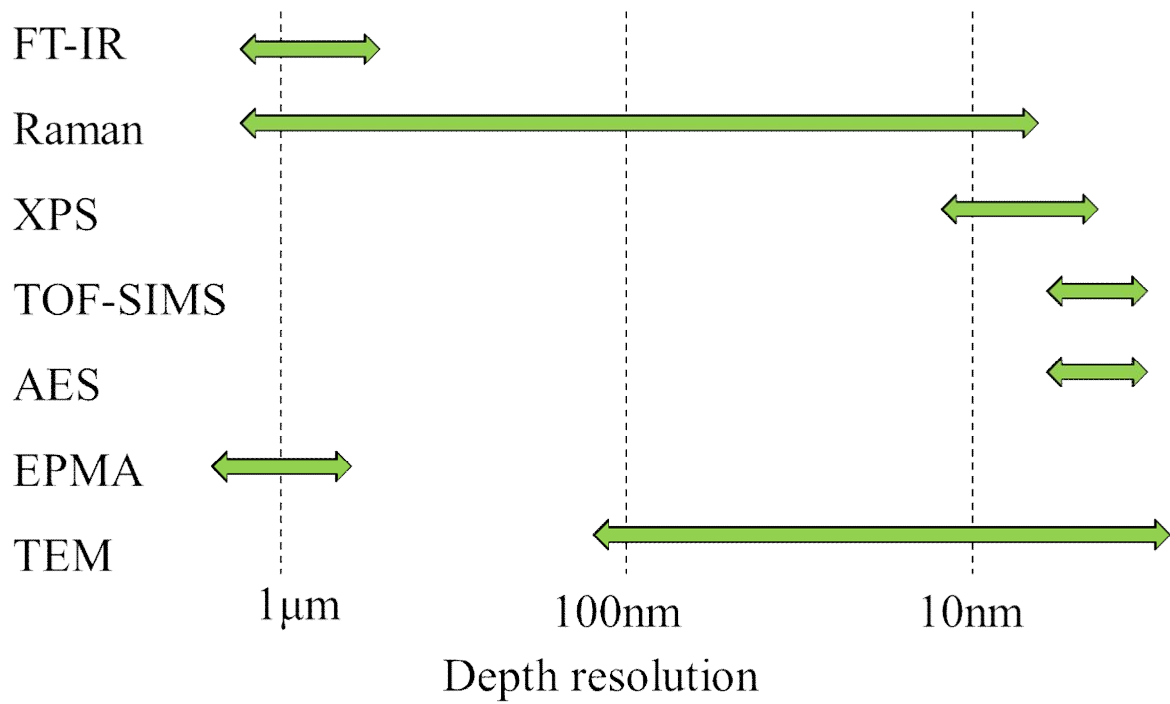

Fig. 1-2. Depth resolution for each analytical method

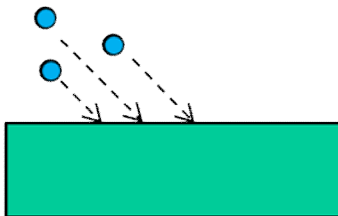

Fig. 1-3. Depth analysis of organic film using FT-IR

■Analysis in depth direction by repeating polishing and ATR measurement.

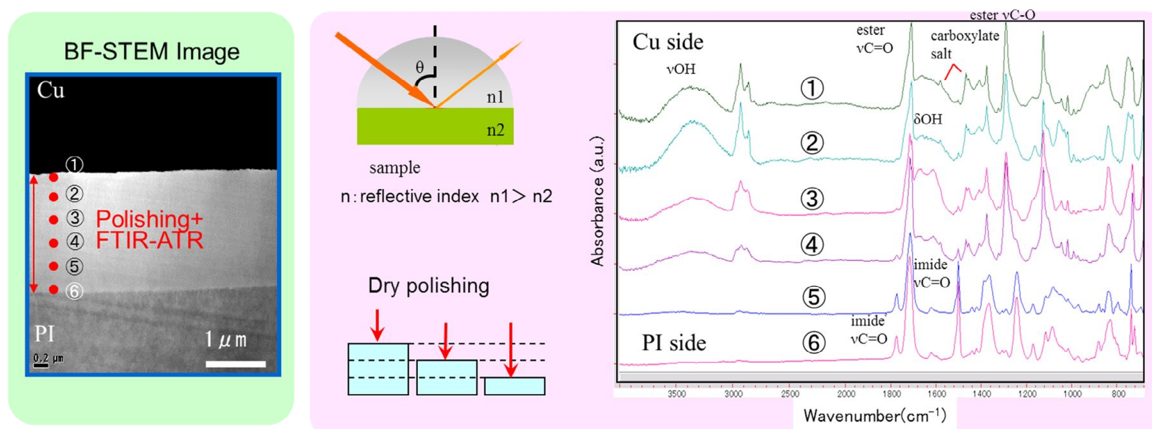

・It is presumed that the interfacial layer is an aromatic ester adhesive.

・The amount of carboxylate salt and OH groups in the adhesive is large on the Cu side.

→It appears that the reaction (the hydrolyzation of the ester groups) of NiCr plating or Cu and the adhesive occurred.

Fig. 1-4. Depth analysis by repeating polishing and ATR measurement

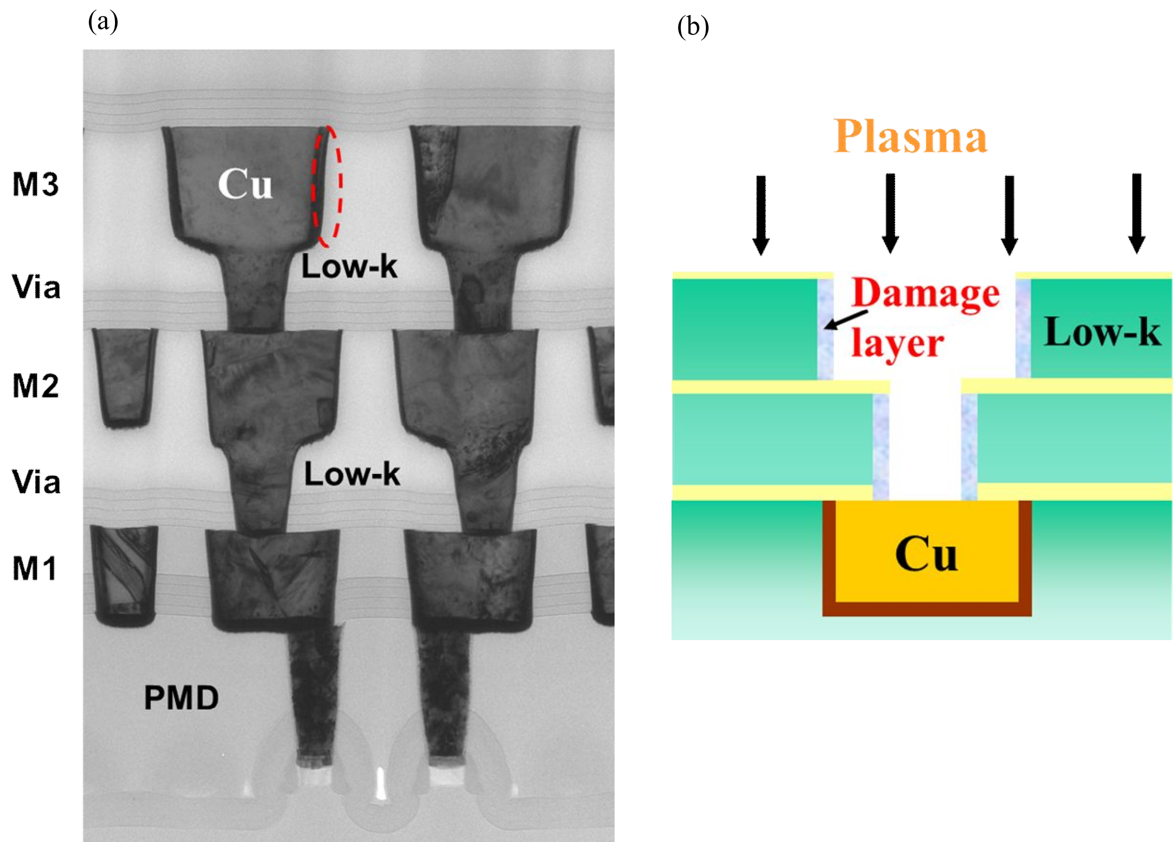

Fig. 1-5. (a) TEM cross section image of commercial device. (b) Schematic view of trench formation process.

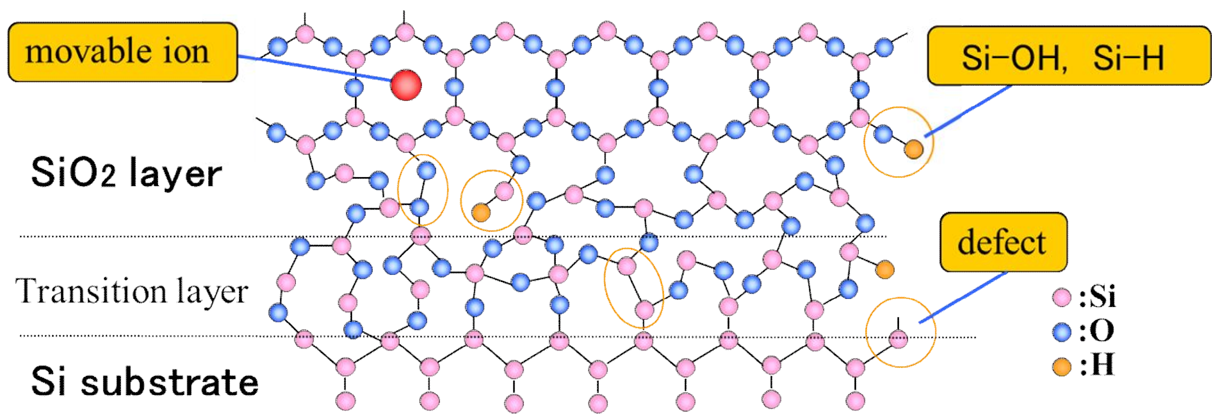

Fig. 1-6. Schematic view of SiO_2/Si interface

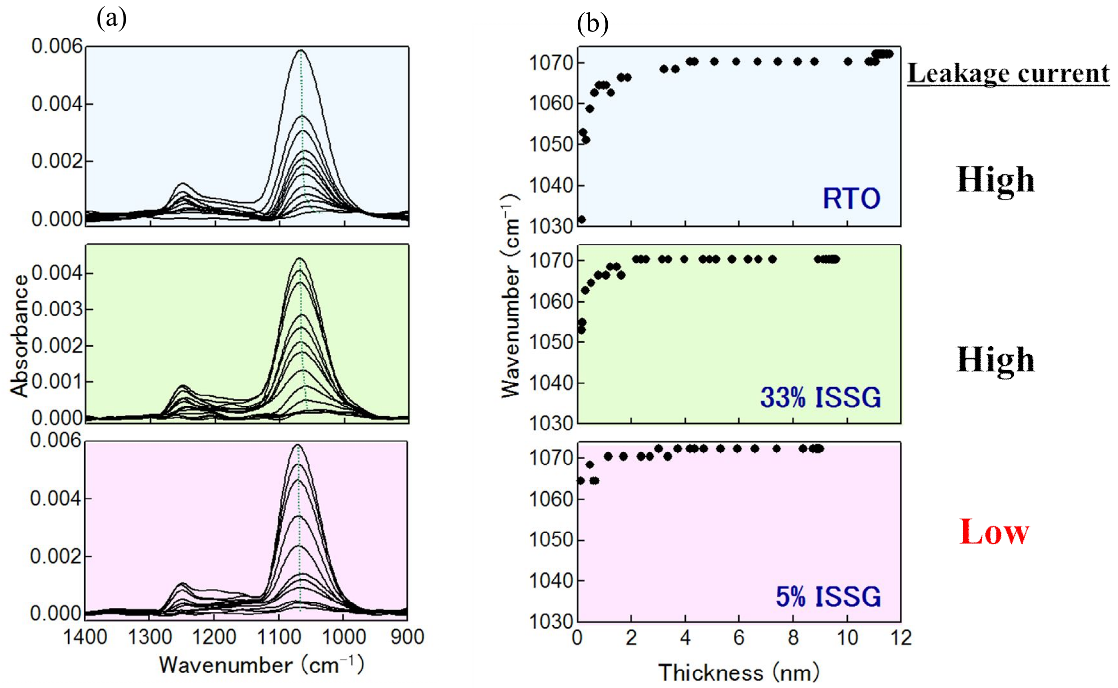

Fig. 1-7. (a) Depth profile spectra for 9-nm SiO_2 film which exhibited different electrical properties. (b) Si–O peak positions as a function of SiO_2 thickness

Chapter 1

Characterization of Ashing Damage in Depth in Low-k Dielectric Films by Microscopic IR Method

ABSTRACT

The author developed special pretreatment for the depth analysis and investigated the ashing damages of low-k films in the depth direction by the gradient shaving preparation (GSP) using the microscopic IR method. Ashing processes were performed on the MSQ films on Si substrates under conditions in which a fixed amount of resist was removed using O_2, NH_3, and He/H_2 gases. The Si-CH_3 bond decreased from only the surface area to a depth of approximately 100 nm in the NH_3 ashing, whereas, in the O_2 ashing, there is an extremely low level of concentration over the entire depth. Further, a change in the structure of the Si-O network occurred. On the other hand, in the He/H_2 ashing, no change in the film structure was observed. Microscopic FT-IR with GSP is useful technique to characterize chemical structure in depth direction for thin low-k film.

INTRODUCTION

Advanced ultra-large-scale integration (ULSI) requires the replacement of a SiO_2 (k = 4.1) dielectric interlayer material with one that has a lower dielectric constant, in order to prevent signal delay. Low-k films have recently been used as interlayer dielectric materials for advanced Cu/low-k interconnects[1-5]. MSQ (methyl silsequioxane) is one possible low-k material for use as a replacement. However, MSQ is more susceptible to changes in its structure by treatments such as dry etching or ashing processes compared to more conventional SiO_2 materials. Treatment via one of these processes induces an increase in the dielectric constant and/or degradation with regard to the hygroscopic properties. Therefore, it is important to gain knowledge about the quality and origin of the process-induced damage and the depth of the damage to improve these manufacturing processes. Fourier transform infrared (FT-IR) analysis easily reveals the chemical bonding structure of porous low-k films in a quantitative manner, and it does not affect the film properties during spectral measurements;[2,3] as such, FT-IR has been used in previous studies on low-k films.[5-15] Furthermore, FT-IR is an effective tool for characterizing a blanket low-k film processed via various plasma treatments. However, it is difficult to evaluate the depth of a chemical bonding structure in sub-micron thickness low-k thin films, and structural changes in the depth direction have not yet been reported. Here, we have developed a new pretreatment method for evaluating chemical bonding in the depth direction for such thin films, and evaluated the chemical structural changes in this direction in low-k dielectric films after several ashing processes using a GSP method with microscopic IR techniques.

EXPERIMENTAL DETAIL

250-nm thick porous MSQ films (k = 2.3) were prepared on Si (100) substrates, and subsequently, the ashing processes were performed on the MSQ films under conditions in which a fixed amount of resist was removed using O_2, NH_3, and He/H_2 gases. A Si substrate with more than 1 Ωcm resistivity was used in this study. IR light passes through this substrate, and therefore, transmittance measurements can be carried out. The ashing damage to the MSQ films was characterized by Fourier transform infrared spectroscopy (FT-IR), X-ray photoelectron spectroscopy (XPS), Rutherford back scattering/Hydrogen forward scattering spectrometry (RBS/HFS), and Raman spectroscopy techniques. Obtained information for each analysis was shown in Table 2-1. The FT-IR measurement in depth was performed by line-scanned transmittance measurements for the slope processed by the gradient shaving preparation (GSP) using the microscopic IR method, as shown in figure 2-1 [16].

GSP is a mechanical pretreatment method that does not use water and/or solution, or argon ions etc. Therefore, the low-k film does not suffer the damages under this pretreatment process. The slope obtained by GSP is more than 1000 times that of the thickness of low-k films. Information on the depth direction of the film can be obtained by some line-scanned surface analytical techniques. The information regarding a certain depth is acquired when the IR beam is used as an analytical probe from the obtained difference in adjacent measurement positions. Therefore, depth profile spectra were obtained by the subtraction of each raw spectrum from the next one.

RESULTS AND DISCUSSION

Changes in the dielectric constant by ashing

The dielectric constants of low-k films were measured by the mercury probe. Obtained dielectric constant of MSQ films were shown in table 2-2. No change in the dielectric constant by the He/H_2 ashing was observed. On the other hand, by the O_2 and NH_3 ashing, an increase was observed in the dielectric constant by approximately 42.6% and 13.9%, respectively [17]. In the view of electrical property, O_2 and NH_3 ashing cause process induced damage for low-k film and He/H_2 ashing cause no damage for low-k film.

Change of chemical structure in depth by ashing

Figure 2-2 shows the IR transmission spectra of the MSQ films. The $Si\text{-}CH_3$ band appeared at 1260 cm^{-1} and decreased in the NH_3 and O_2 ashing.[3] The degree of change is relatively minor in NH_3 ashing as compared to O_2 ashing. Furthermore, the Si-OH band appeared around 950 cm^{-1}, which indicated that the MSQ film might tend to absorb moisture in the NH_3 and O_2 ashing. The Si-H band appeared at 900 cm^{-1} and increased in the NH_3 and He/H_2 ashing. It is presumed that the terminal functional groups of the Si-O network changed by ashing. In case of He/N_2 ashing, there is no damage in electrical property. However, Si-H groups increased by the ashing. Si-H groups might not have any effect for electrical property.

Figure 2-3 shows the depth profile spectra obtained by the microscopic IR measurements. The upper spectra in each figure are those of the surface, and the lower spectra are those of the interface in the MSQ film. Each spectrum contained information pertaining to the MSQ films for a depth of 25 nm. In the reference sample (c), no change in the spectrum was observed in the depth direction. However, in the case of O_2 (a) and NH_3 (b) ashing, changes in the spectrum in the depth direction were observed. The spectrum at the interface after the

NH_3 ashing showed a shape similar to that of the reference. On the other hand, it was found that a peak position for the Si-O stretching mode appeared around 1049 cm^{-1} near at the interface and was shifted to a small extent to 1064 cm^{-1} at the surface area. This implies that the structure of a Si-O network, which is the primary network in the MSQ film, changes near the surface by the NH_3 ashing.

In the O_2 ashing, the peak position for the Si-O stretching around 1073 cm^{-1} at the interface was shifted to a small extent to 1080 cm^{-1} near the surface area. The Si-O peak positions were blue-shifted compared with NH_3 ashing and reference. The Si-O peak position of low-k films tends to blue-shift due to Si-O network cross linkage progressing. It is presumed that the MSQ film transformed into a SiO_2 like structure in entire film in O_2 ashing and on the surface of low-k film in NH_3 ashing.

Figure 2-4 shows the depth profile of the ratios of the peak intensity of the 1260 cm^{-1} Si-CH_3 band to the peak intensity of the Si-O band. It indicated that the Si-CH_3 bond decreased from only the surface region to a depth of approximately 100 nm in the NH_3 ashing, whereas, in the O_2 ashing, there is an extremely low level of concentration over the entire depth. On the other hand, no change in the amount of Si-CH_3 in the depth direction was observed in the He/H_2 ashing.

Changes in the composition of MSQ films by ashing

Tables 2-3 and 2-4 show the composition of MSQ films characterized by the RBS/HFS and XPS. RBS/HFS gave the composition of MSQ films as a bulk property, whereas XPS gave the composition at the surface of MSQ films. The decrease in the amount of carbon and hydrogen and the increase in the amount of oxygen in the MSQ film in the O_2 and NH_3 ashing can be observed. Nitrogen existed in the surface of the MSQ film in the NH_3 ashing. From these results, it can be deduced that the methyl group disappeared in the ashing process.

Changes in the Si-O network of MSQ films by ashing

Figure 2-5 shows the Raman spectra of the MSQ films. The Peaks were assigned a 4-fold ring structure of the Si-O and/or random network of the SiO_2 at 500 cm^{-1} and a 3-fold ring structure of Si-O at 610 cm^{-1}. As the ashing damage increased, the 600 cm^{-1} band intensity decreased and the peak shape of 500 cm^{-1} band changed. Therefore, it is presumed that the Si-O network changes by O_2 and NH_3 ashing. [18]

The mechanism of degradation of low-k film by O_2 and NH_3 ashing

According to FT-IR results, the Si-CH_3 bond decreased from only the surface region to a depth of approximately 100 nm in the NH_3 ashing and there is an extremely low level of concentration over the entire depth in the O_2 ashing. XPS and RBS/HFS results show the methyl group disappeared in the ashing process. Therefore, it is concluded that ashing damage in the low-k film is caused by breaking of Si-CH_3 groups. Disappearing of Si-CH_3 group causes dangling bonds in the low-k film. The dangling bonds are unstable and Si-OH groups generate with reacting moisture in the atmosphere. The generated Si-OH groups also draw the moisture. The dielectric constant of water is approximately 80, larger than that of low-k film. Therefore, decreasing of Si-CH_3 groups in the low-k film generates degradation of dielectric constant. It is presumed that the amount of Si-CH_3 changes correlated with dielectric constant of the low-k film.

CONCLUSION

We investigated the ashing damages of low-k films in the depth direction by the gradient shaving preparation (GSP) using the microscopic IR method and the ashing damages to the MSQ films were characterized in the depth direction.

The Si-CH_3 bond decreased from only the surface area to a depth of approximately 100 nm in the NH_3 ashing, whereas, in the O_2 ashing, there is an extremely low level of concentration over the entire depth. It was shown that in the NH_3 and O_2 ashing, the methyl group disappeared from the surface area and a change occurred in the structure of the Si-O network. On the other hand, after the He/H_2 ashing, no change in the film structure was observed. It is concluded that ashing damage in the low-k film is caused by breaking of Si-CH_3 groups. Decreasing of Si-CH_3 groups in the low-k film generates degradation of dielectric constant. It is presumed that the amount of Si-CH_3 change correlated with dielectric constant of the low-k film.

The result from our study showed that the change in the film structure and the extent of ashing damage in the depth direction depends on the ashing conditions.

Microscopic FT-IR with GSP is useful technique to characterize chemical structure in depth direction for thin low-k film.

REFERENCES

[1]R.D. Goldblatt, B. Agarwala, M.B. Anand, E.P. Barth, G.A. Biery, Z.G. Chen, and S. Gohen: Proc. of IITC. 1, (2000), pp. 261-263.

[2]A. Grill, J. Appl. Phys. 93, 1785 (2003).

[3]A. Grill and D.A. Neumayer, J. Appl. Phys. 94, 6697 (2003).

[4]B. Zhao and M. Brongo, Mater. Res. Soc. Symp. Proc. 565, 137 (1999).

[5]J.-N. Sun, D.W. Gidley, T.L. Dull, W.E. Frieze, A.F. Yee, E.T. Ryan, S. Lin, and J. Wetzel, J. Appl. Phys. 89, 5138 (2001).

[6]C. Himcinschi, M. Friedrich, S. Fruhauf, S.E. Schulz, T. Gessner, and D.R.T. Zahn, Thin Solid Films. 455-456, 433 (2004).

[7]M. Albrecht and C. Blanchette, J. Electrochem. Soc. 145, 4019 (1998).

[8]S. Sugahara, T. Kadoya, K. Usami, T. Hattori, and M. Matsumura, J. Electrochem. Soc. 148, F120 (2001).

[9]B.C. Transferetti, C.U. Davanzo, and M.A. Moraes, Macromolecules. 37(2), 459 (2004).

[10]C.Y. Wang, J.Z. Zheng, Z.X. Shen, Y. Lin, and A.T.S. Wee, Thin Solid Films. 397, 90 (2001).

[11]C. Y. Wang, Z. X. Shen, and J. Z. Zheng, Applied Spectroscopy. 54, 209 (2000).

[12]Yoon-Hae Kim, Seok-Kiu Lee and Hyeong Joon Kim, J. Vac. Sci. Technol. A 18, 1216 (2000).

[13]Yoon-Hae Kim, Moo Sung Hwang, Hyeong Joon Kim, Jin Yong Kim and Young Lee, J. Appl. Phys. 90, 3367 (2001).

[14]J. Lubguban Jr., T. Rajagopalan, N. Mehta, B. Lahlouh, S. L. Simon and S. Gangopadhyay, J. Appl. Phys. 92, 1033 (2002).

[15]Yee Wee Koh, Kian Ping Loh, Liu Rong, A. T. S. Wee, Liu Huang and J. Sudijono, J. Appl. Phys. 93, 1241 (2003).

[16]N. Nagai, T. Imai, K. Terada, H. Seki, H. Okumura, H.Fujino, T. Yamamoto, I. Nishiyama, A. Hatta, Surface and Interface Analysis. 33, 545 (2002).

[17]A. Matsushita et al, Proceedings IITC 2003, 147 (2003).

[18]Hilton G.Pryce Lewis et al, J. Electrochem. Soc. 148, F212 (2001).

Table. 2-1. Characterized targets of each analytical techniques for low-k films.

Analytical technique	Characterized target
IR (transmission)	Chemical bonding structure (entire film)
XPS (X-ray photoelectron spectroscopy)	Composition (surface)
RBS/HFS (Rutherford back scattering Hydrogen forward scattering)	Composition (entire film)
Microscopic IR with GSP	Depth profile of chemical bonding structure

Table. 2-2. The dielectric constant after ashing with various types of gases.

Ashing gas	Dielectric constant
O_2	3.6
NH_3	2.9
He/H_2	2.3
Ref	2.3

Table. 2-3. Composition of the Low-k films by RBS/HFS.

	C/Si	**O/Si**	**H/Si**
O_2 ashing	0.19	2.05	0.31
NH_3 ashing	0.59	1.91	1.45
He/H_2 ashing	0.77	1.89	1.60
Ref	0.77	1.89	1.60

Table. 2-4. Composition of the surface of MSQ films by XPS (atomic %)

	C	**O**	**N**	**Si**	**F**	**C/Si**	**O/Si**
O_2 ashing	3.3	67.5	-	28.6	0.6	0.12	2.36
NH_3 ashing	4.7	65.6	2.2	27.5	-	0.17	2.39
He/H_2 ashing	15.9	55.8	-	28.3	-	0.56	1.97
Ref	17.1	55.2	-	27.7	-	0.62	1.99

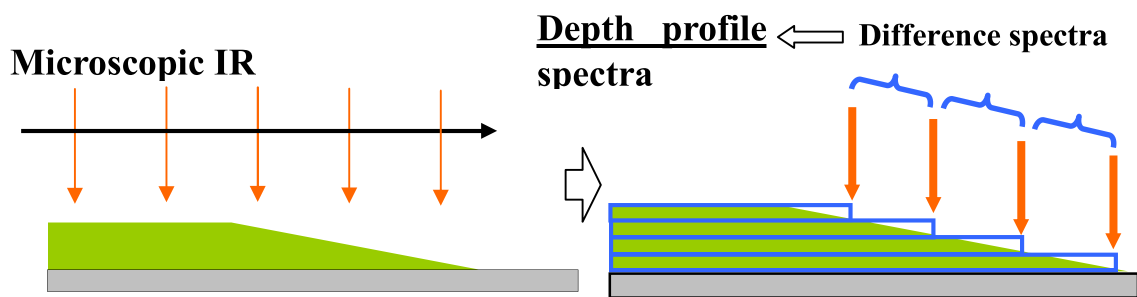

Fig. 2-1. Principle of the depth profile analysis by microscopic IR.

MSQ film is mechanically shaved with a slope and line-scanned IR measurements were performed to obtain the depth direction after ashing with various types of gases. Line scan was performed using microscopic IR to obtain the slope.

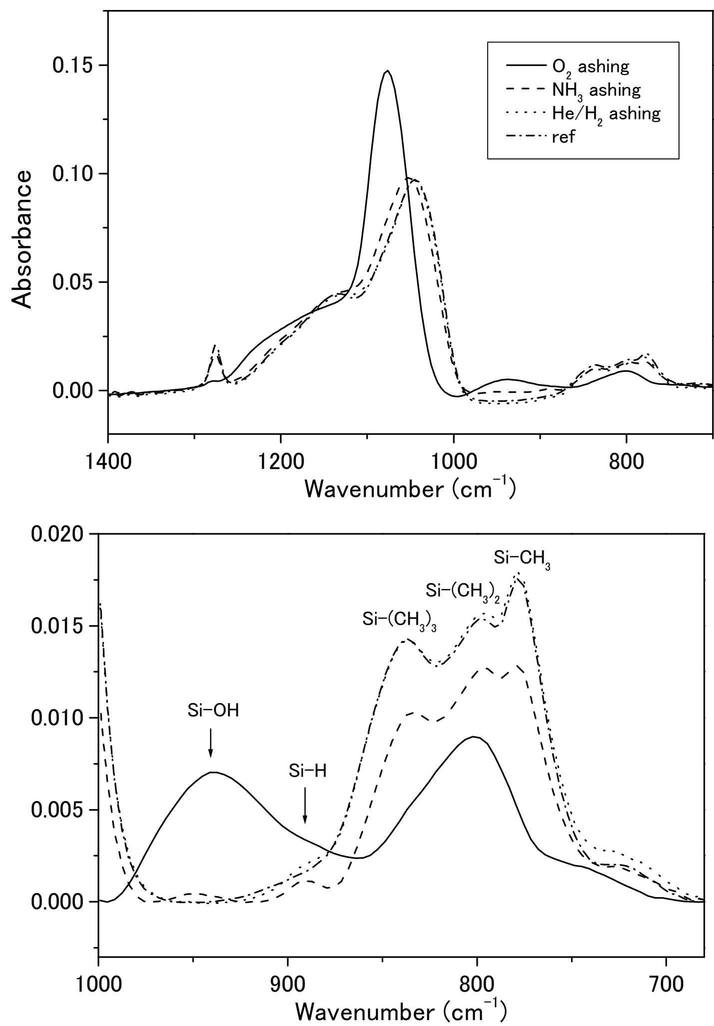

Fig. 2-2. IR absorption spectra of MSQ films in different ashing conditions.

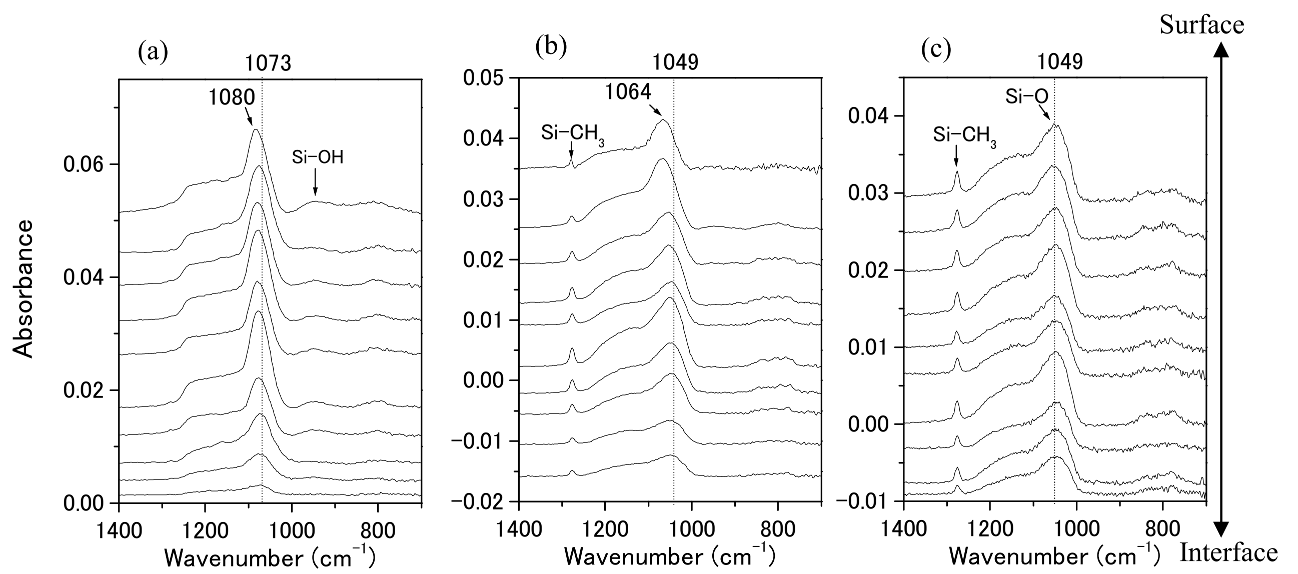

Fig. 2-3. Depth profile spectrum of MSQ films.

(a) O_2 ashing; (b) NH_3 ashing; (c) Reference.

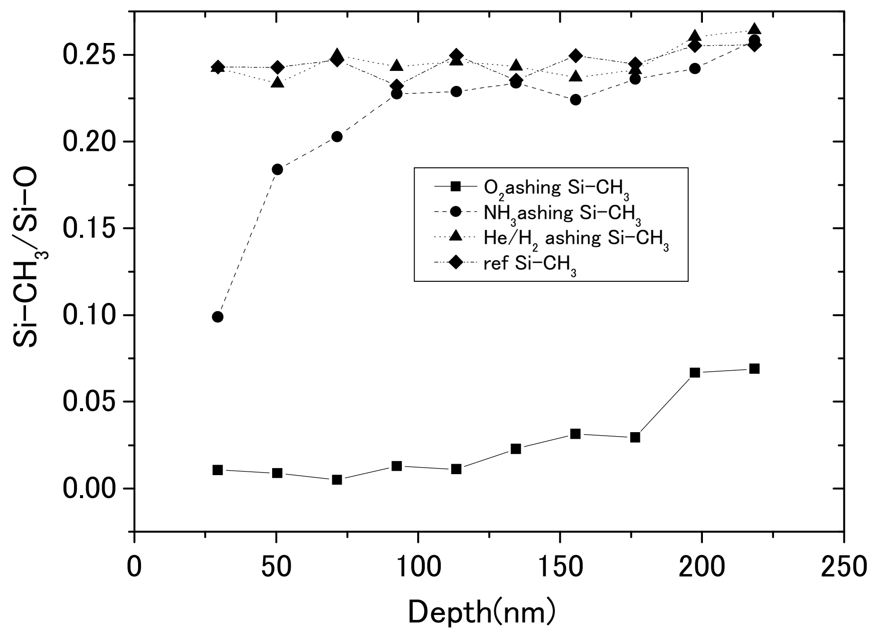

Fig. 2-4. Depth direction distribution of Si-CH_3 in the MSQ film.

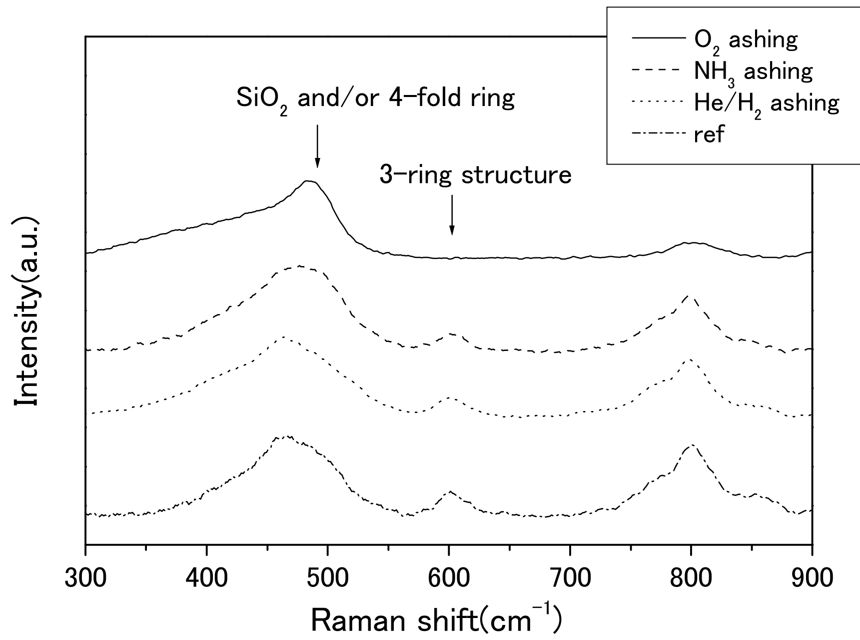

Fig. 2-5. Raman spectra of MSQ films in different ashing conditions.

Chapter 2

Characterization of process-induced damage in Cu/low-k interconnect structure by microscopic infrared spectroscopy with polarized infrared light

ABSTRACT

Microscopic Fourier-transform infrared (FT-IR) spectra are measured for a Cu/low-k interconnect structure using polarized IR light for different widths of low-k spaces and Cu lines, and for different heights of Cu lines, on Si substrates. Although the widths of the Cu line and the low-k space are 70 nm each, considerably smaller than the wavelength of the IR light, the FT-IR spectra of the low-k film were obtained for the Cu/low-k interconnect structure. A suitable method was established for measuring the process-induced damage in a low-k film that was not detected by the TEM-EELS (Electron Energy-Loss Spectroscopy) using microscopic IR polarized light. Based on the IR results, it was presumed that the FT-IR spectra mainly reflect structural changes in the sidewalls of the low-k films for Cu/low-k interconnect structures, and the mechanism of generating process-induced damage involves the generation of Si-OH groups in the low-k film when Si-CH_3 bonds break during the fabrication processes. The Si-OH groups attract moisture and the OH peak intensity increases. It was concluded that the increase in the OH groups in the low-k film is a sensitive indicator of low-k damage. We achieved the characterization of the process-induced damage that was not detected by the TEM-EELS and speculated that the proposed method is applicable to interconnects with line and space widths of 70 nm/70 nm and on shorter scales of leading edge devices. The location of process-induced damage and its mechanism for the Cu/low-k interconnect structure were revealed via the measurement method.

INTRODUCTION

As mentioned previously in Chapter 1, low-k films are more susceptible to structural and chemical changes during manufacturing processes such as dry etching, ashing, and barrier metal deposition.[1-3] These processes can cause deterioration that leads to increased dielectric constants and/or degradation of the films' hygroscopic properties. Such damage can have an adverse effect on the performance and reliability of Cu/low-k interconnects.

To evaluate process-induced damage, electron energy loss spectroscopy (EELS) equipped to a low-voltage transmission electron microscope (TEM) has been used for the precise characterization of process-induced damage in low-k interconnect dielectrics; in addition, decreased amounts of carbon in the trench walls due to dry etching has also been previously reported.[4] However, the obtained results featured less information about the detailed chemical bonding structure, and it is difficult to characterize low-k materials without incurring electron beam damage that is inherent to TEM.

In Chapter 1, line analysis was used with a microscopic IR method against the inclined surface formed by special pretreatment, and the chemical bonding structure in the depth direction was obtained.[5] Information regarding chemical bonding structure changes and the depth at which they occur is useful for improving manufacturing processes related to low-k films. However, the actual low-k film is processed into a trench structure, and damage may primarily occur in the low-k film trench side walls. The process-induced damage on the blanket film and on the side wall in the Cu/low-k interconnect structure may differ even under the same plasma conditions. In addition, any IR radiation is shielded when forming a Cu wiring on the low-k film, preventing the use of IR characterization in evaluating this issue. To characterize sheer process damage, it is important to evaluate Cu/low-k interconnect structures. Thus, the possibility of characterizing damage in narrow low-k spaces between Cu

lines less than 100 nm was investigated using a microscopic FT-IR method.[6, 7]

In the present study, the process-induced damage is negligible and is difficult to characterize using TEM-EELS. Therefore, a microscopic FT-IR method was explored as a suitable measurement method for characterizing process-induced damage in Cu/low-k interconnect structures. Damage layer analysis was carried out using this FT-IR method for samples with different line and space widths and different line heights. Furthermore, the locations where damage is detected by this method and the processed-induced damage mechanisms were discussed. Finally, the locations where process-induced damage occurs and its mechanisms in a Cu/low-k interconnect structure were revealed.

EXPERIMENTAL DETAIL

A porous SiOC low-k film with k = 2.5 was used for the experiment. A SiOC film consists of a Si-O network and Si-CH_3, Si-H groups. The sample structure used in the microscopic FT-IR measurements is shown in Fig. 3-1. The sample structure is appropriate for FT-IR measurements and it is easy to determine the location of the process-induced damage. A Si substrate with more than 1 Ωcm resistivity was used in this study. IR light passes through this substrate, and therefore, transmittance measurements can be carried out. A 30-nm-thick SiC film was deposited on the silicon substrate and a 200-nm-thick porous SiOC film was deposited on the SiC film. Cu narrow line structures were made by plasma trench etching using fluorocarbon gas, Cu electroplating, and Cu chemical mechanical polishing (Cu-CMP). Finally, Cu narrow line structures were formed in an area of 100 μm^2 for every same line and space structures.

The FT-IR spectra were measured using the transmittance mode in a Fourier transform spectrometer (Perkin Elmer Spotlight 300) with an IR polarizer to generate p- or s- polarized IR light. The measurements were performed in an area of 100 μm^2 by focusing IR light with an aperture, as shown in Fig. 3-2. To decide a suitable FT-IR method for the assessment of process-induced damage, the effect of the direction of the electric field under IR light on the direction of the Cu line is discussed.

To investigate the area where process-induced damage was detected in the Cu/low-k structures, structural samples with different widths of the low-k spaces (S) and the height of the Cu lines (T) were investigated. We formed samples with different widths for the low-k spaces and Cu lines (L). Figure 3-3 shows the top view of the schematic Cu/low-k line and space structure with different space widths. The Cu line widths were 70 nm. In this study, line occupancy is defined as the ratio of the occupied area of a Cu line to the total area of Cu

lines and low-k spaces. The line occupancies were 10%, 15%, 30%, and 50%. In a different case, L and S were fixed at 70 nm, and T was varied to three different lengths: standard (100 nm), tall (125 nm), and short (75 nm).

RESULTS AND DISCUSSION

Figure 3-4 shows the IR transmittance to a Si substrate for L/S = 70/70 nm measured using different polarized IR light whose electric field component is (a) parallel and (b) perpendicular to the Cu lines. When the electric field component of the IR light was parallel to the Cu lines, the transmittance of IR light was less than 10%. In contrast, when the electric field component of the IR light was perpendicular to the Cu lines, the transmittance was almost 100%. This indicates that the Cu narrow lines work as an IR polarizer and only the electric field component of the IR light perpendicular to the Cu lines can pass through the Cu/low-k interconnect structure. The transmittance is observed to slightly exceed 100%. This phenomenon is considered to be caused by the refractive effect of IR through a silicon wafer with/without deposited films. Therefore, we determined a suitable measuring method that uses IR light whose electric field component is perpendicular to the Cu lines.

Figure 3-5 shows the IR spectra of a blanket film (non-patterning) and patterning samples (L/S = 70: 70 nm). The IR measurements were carried out using polarized IR light. The spectral shapes are similar to each other. It is very likely that the effect of Cu lines is non-existent, and thus, we can measure the Cu/low-k interconnect structure. The assignments of the main peaks of the low-k film are summarized in Table 3-I[5, 8-11].

Figures 3-6(i) and (ii) display microscopic FT-IR spectra in the (i) 4000–700 cm^{-1} and (ii) 3800–2600 cm^{-1} regions for Cu/low-k samples with different spaces and line widths, respectively (Fig. 3-3). Each obtained spectrum reflects a different volume of low-k film components. Thus, we use the relative intensity of a band to the intensity of a band at 1050 cm^{-1} owing to the Si-O stretching mode, which is the main framework in the low-k film. The relative intensities of the bands due to the $Si\text{-}CH_3$, Si-H, and OH stretching modes ($Si\text{-}CH_3$: 1270 cm^{-1}, Si-H: (2240 and 2180) cm^{-1}, OH: 3400 cm^{-1}) to that of the 1050 cm^{-1} band are

shown in Fig. 3-7(i), (ii). The Si-OH peaks also appeared at approximately 900 cm^{-1} [9-12] and are easily distinguishable from those owing to the OH groups derived from water. However, in the case of the low-k film, the peak of the Si-H bands is located around the same wavenumber as shown in Table 3-I. Thus, the peak intensity of the OH groups was estimated as the sum of the OH and the Si-OH peak area. The Si-H/Si-O intensity ratio is almost the same for all samples; however, the Si-CH_3/Si-O intensity ratio decreases gradually as the space width decreases. In addition, the OH/Si-O ratio significantly increases as the space width decreases. According to our previous report, the amount of Si-CH_3 groups decreased and its structure changed to a SiO_2 network structure owing to the plasma processes[23]. It appears that the generation of OH groups is related to process-induced damage; the volume fraction of the sidewall in the low-k film increases for narrower low-k space width.

Figure 3-8 shows the Si-O peak intensity obtained from Fig. 3-6. The absorption intensity of Si-O increases as the width of the low-k space reduces. This phenomenon appears to be due to an increase in the Si-O cross-linkage, as a result of process-induced damage. However, it is also likely that a localized electric field is generated between the Cu lines by the IR light. It may be caused by the surface-enhanced infrared absorption (SEIRA) phenomenon that has been reported so far[13-16]. The IR absorption of adsorbed species on gold, silver, and copper island films is enhanced; the degree of enhancement depends on the size of the islands and the gaps between islands. Thus, the Si-O peak intensity might be enhanced by SEIRA, and it might enable the sensitive detection of process-induced damage.

Figures 3-9(i) and (ii) depict microscopic FT-IR spectra in the (i) 1400–700 cm^{-1} and (ii) 3900–2600 cm^{-1} regions of the samples with different T (line and space widths of 70 nm) values. The T value is changed to three different heights—standard (100 nm), tall (125 nm), and short (75 nm)—to confirm the location of the damage in the low-k film. The relative peak intensities of Si-CH_3, Si-H, and OH bands to that of the Si-O band at 1050 cm^{-1} are

shown in Fig. 3-10(i) and (ii). As T increases, the relative peak intensity of the OH groups increases. The number of OH groups was shown to correlate with the length of the side walls. We concluded that FT-IR spectra reflect mainly the structural changes such as process-induced damage in the sidewall of a low-k film.

It is presumed that the OH groups are generated in the low-k film when Si-CH_3 bonds break during the fabrication processes, and they are derived from atmospheric moisture, as shown in Fig. 3-11. As mentioned previously, process-induced damage was occurred in the side wall of low-k films, and the amount of Si-CH_3 groups decreased. However, the difference in the amount of the total Si-CH_3 groups before and after the damage is small because there are many Si-CH_3 groups in the low-k films. The Si-OH groups are negligible in the initial low-k film. Si-OH groups that were generated by the process-induced damage also draw moisture. Therefore, the total amount of OH groups is apparently amplified by the adsorption of water.

We attempted to evaluate the amount of carbon by EELS equipped with a low-voltage TEM. The measurement method is shown in Ref. 8. The carbon concentration mapping using EELS at the C-K edges is shown in Figure 3-12. If the depletion of carbon occurred in the sidewall of the low-k film, the color of the area would be denser than the other areas of the low-k film. However, the depletion of carbon was not clearly observed. The carbon detection limit of the TEM-EELS is approximately 0.5%. The composition errors were estimated to be ±2% and the space resolution was approximately 1 nm for the TEM-EELS. However, we detected Si-OH peaks by the FT-IR measurement for the same sample. The FT-IR can measure several sidewalls of the low-k films simultaneously and the Si-OH peak intensity is apparently amplified by the adsorption of water; it enabled a highly sensitive measurement of the process-induced damage for the sidewall of the low-k film and contributed to the revelation that the number of OH groups is a more sensitive indicator for a low-k damage

evaluation. This may affect the reliability of the Cu/low-k interconnects.

CONCLUSION

In the present study, the microscopic FT-IR spectra were measured for a Cu/low-k interconnect structure that had different widths of low-k spaces (S), widths of Cu lines (L), and heights of Cu lines (T) on Si substrates with polarized infrared light.

Based on the IR results, the effect of the direction of the electric field under IR light on the direction of the Cu line was investigated. We developed a suitable damage measuring microscopic FT-IR method using IR light whose electric field component is perpendicular to the Cu lines.

The microscopic FT-IR spectra for Cu/low-k samples with different space and line widths and samples with different T (line and space widths of 70 nm) were investigated. The results show that the process-induced damage that was detected by the FT-IR method is mainly reflected in the structural changes in the sidewall of a low-k film and the number of OH groups correlated with the length of the side walls. It is concluded that FT-IR spectra mainly reflect the process-induced damage in the sidewall of a low-k film.

Based on the discussion about process-induced spectral changes of low-k films, it is considered that the mechanism of generating process-induced damage involves the generation of the OH groups in the low-k film when Si-CH_3 bonds break during the fabrication processes and are derived from atmospheric moisture.

There are many Si-CH_3 groups in the low-k films. However, OH groups are not excited in the low-k film without damage. It was revealed that the number of OH groups was a more sensitive indicator for the low-k damage evaluation of the microscopic FT-IR method. We achieved the characterization of the process-induced damage that was not detected by the TEM-EELS. This may influence the reliability of the Cu/low-k interconnects. The method is applicable to narrow interconnects, e.g., those with line and space widths of 70 nm/70 nm or

less for advanced semiconductor processes.

Thus, the FT-IR study has provided us with novel and unique information regarding process-induced damage in Cu/Low-k interconnect structures.

REFERENCES

[1]N. Posseme, T. Chevolleau, T. David, M. Darnon, O. Louveau, and O. Joubert, J. Vac. Sci. Technol. B 25, 1928 (2007).

[2]X. Hua, M. Kuo, G.S. Oehrlein, P. Lazzeri, E. Iacob, M. Anderle, C.K. Inoki, T.S. Kuan, P. Jiang, and W. Wu, J. Vac. Sci. Technol. B 24, 1238 (2006).

[3]K. Yonekura, K. Yonekura, K. Goto, M. Matsuura, N. Fujiwara and K. Tsujimoto, Jpn. J. Appl. Phys. 44, 2976 (2005).

[4]Y. Otsuka, Y. Shimizu, N. Kawasaki, S. Ogawa, and I. Tanaka, Jpn. J. Appl. Phys. 49, 111501 (2010).

[5]H. Seki, K. Inoue, N. Nagai, M. Shimada, K. Inukai, H. Hashimoto, and S. Ogawa, Proc. AMC. 2004, pp. 375-380.

[6]S. Ogawa, H. Seki, Y. Otsuka, S. Nakao, Y. Takigawa, and H. Hashimoto, Proc. IITC, 2008, pp. 76-78.

[7]H. Seki, N. Tarumi, Y. Shimizu, Y. Otsuka, H. Hashimoto, and S. Ogawa, Proc. AMC, 2008, pp. 647-650.

[8]A. Grill and D.A. Neumayer, J. Appl. Phys. 94, 6697 (2003).

[9]C.Y. Wang, J.Z. Zheng, Z.X. Shen, Y. Lin, and A.T.S. Wee, Thin Solid Films. 397, 90 (2001).

[10]W.A. Pliskin, J. Vac. Sci. Technol. 14, 1064 (1977).

[11]K. M. Davis, M. Tomozawa, J. Non-Cryst. Solids. 201, 177 (1996).

[12]S. Sugahara, T. Kadoya, K. Usami, T. Hattori, and M. Matsumura, J. Electrochem. Soc. 148, F120 (2001).

[13]A. Hartstein, J.R. Kirtley, and J.C. Tsang, Phys. Rev. Lett. 45, 201 (1980).

[14]M. Osawa, Bull. Chem. Soc. Jpn. 70, 2861 (1997).

[15]K. Ataka and J. Herberle, J. Am. Chem. Soc. 125, 4986 (2003).

[16]H. Seki, M. Takada, T. Tanabe, T. Wadayama, and A. Hatta, Surf. Sci. 506, 23 (2002).

Table. 3-I. Peak assignments of an IR spectra of a porous SiOC film.

Peak position(cm^{-1})	Assignments	Comment
3650	ν Si-OH	Due to damage
3300	ν OH	adsorbed water
2970	ν $C-CH_3$	$Si-(CH_3)x$
2240	ν Si-H	$H-SiO_3$
2180	ν Si-H	$H-SiO_2Si$
1640	δ OH	adsorbed water
1410	δ_s $C-CH_3$	$Si-(CH_3)x$
1360	δ $C-CH_2$	$Si-CH_2-Si$
1270	δ_a $C-CH_3$	$Si-(CH_3)x$
1140	ν_a Si-O-Si	Cage
1050	ν_a Si-O-Si	Network
950-900	δ Si-OH	Due to damage
890	δ Si-H	$H-SiO_3$
840	ρ_a CH_3	$Si-(CH_3)_3$
800	ρ_a CH_3	$Si-(CH_3)_2$
780	ρ_a CH_3	$Si-(CH_3)_1$

ν: stretching mode, δ: bending, ρ: rocking, a: anti-symmetric, s: symmetric.

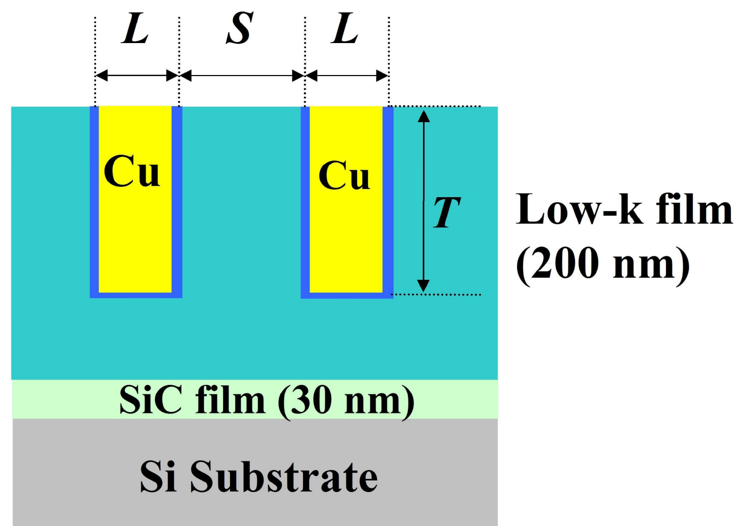

Fig. 3-1 Schematic view of the sample structure. Cu line width (L), low-k space width (S) were changed while keeping Cu line (T) constant, and the height of the Cu lines (T) was changed keeping Cu line width (L) and low-k space width (S) constant.

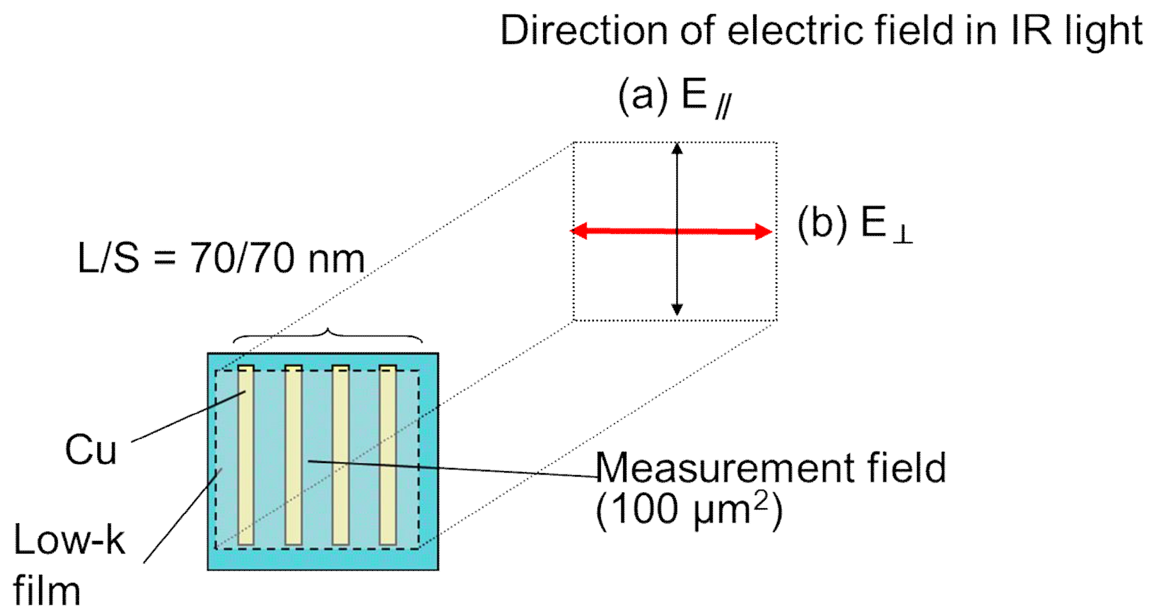

Fig. 3-2 Schematic view of the polarized IR absorption measurement. The electric field component of IR light is (a) parallel and (b) perpendicular to the Cu lines.

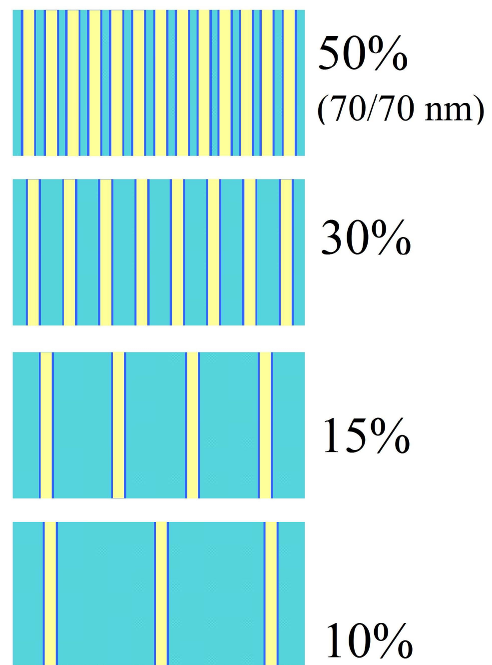

Fig. 3-3 Schematic view of the sample structure with different line occupancies (top view). Line width was fixed at 70 nm and line occupancies were varied: 10%, 15%, 30%, and 50%.

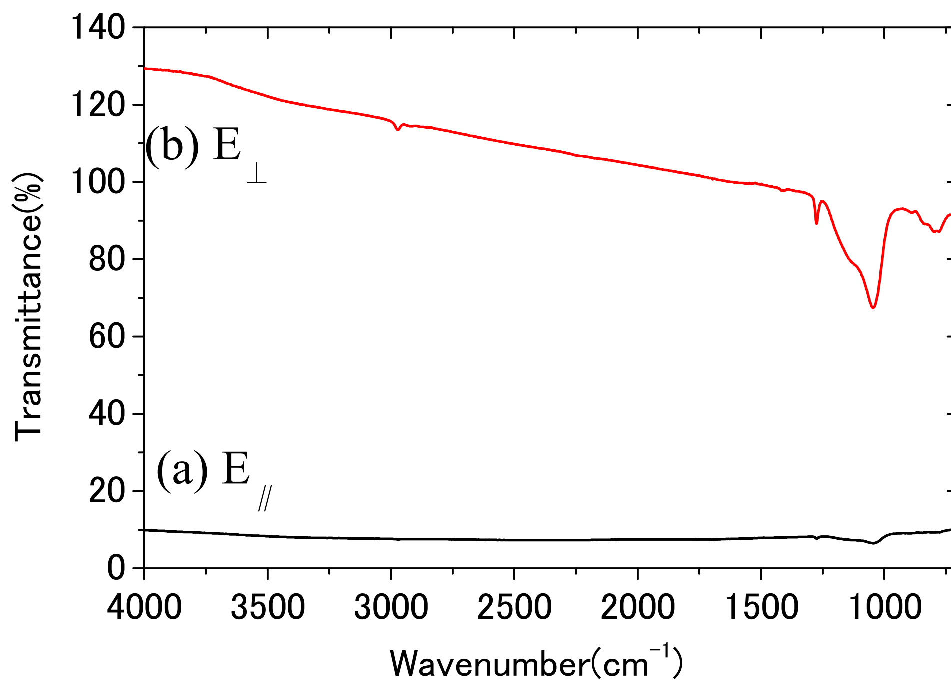

Fig. 3-4 IR transmittance to the Si substrate for L/S = 70/70 nm using different polarized IR light whose electric field component is (a) parallel and (b) perpendicular to the Cu lines.

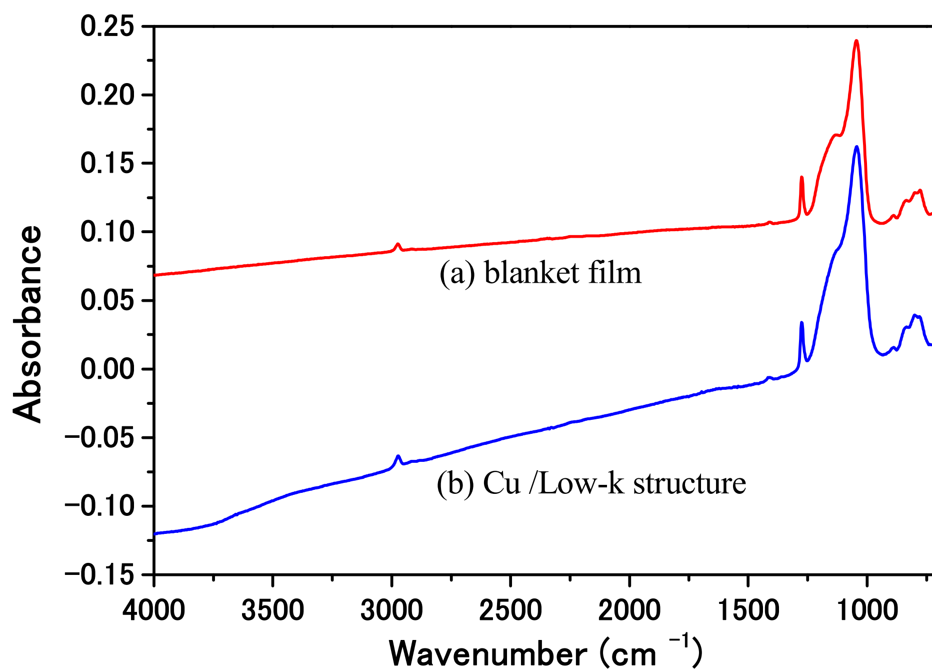

Fig. 3-5 IR spectra of (a) a blanket film and (b) Cu/low-k structure (L/S = 70 nm:70 nm). IR measurements were carried out using polarized IR light.

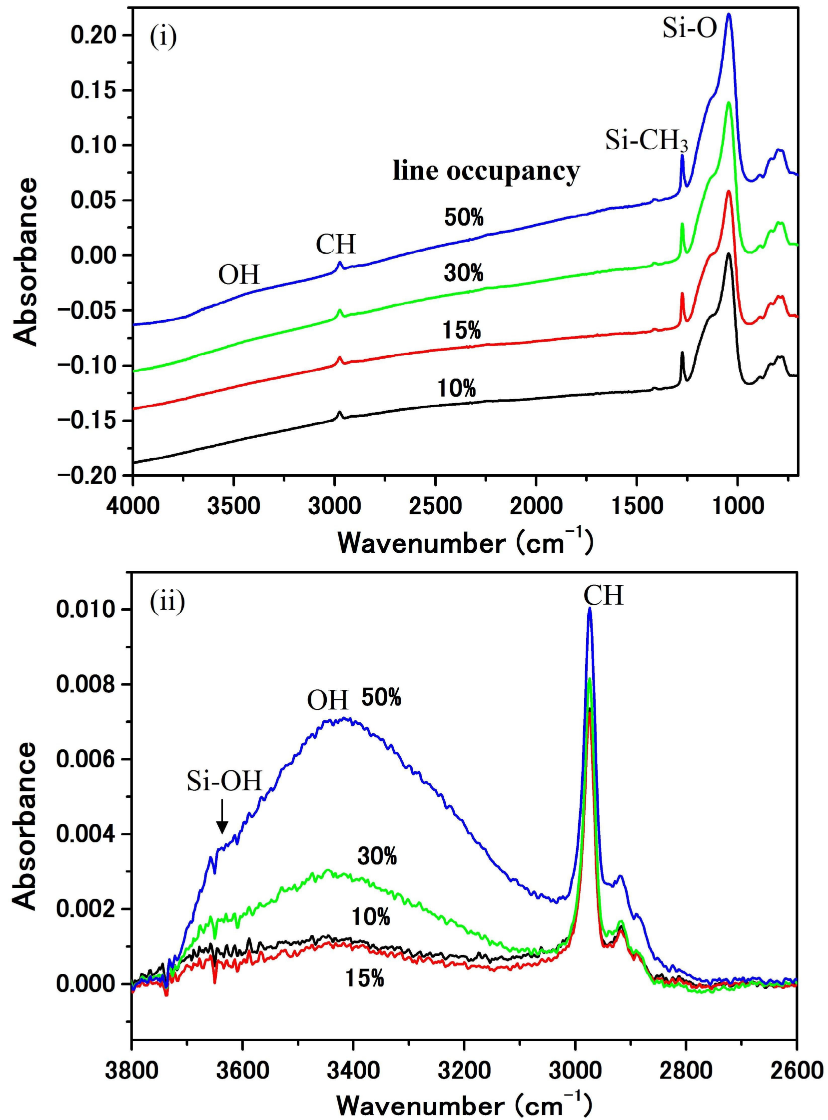

Fig. 3-6 FTIR spectra of Cu/low-k samples with different line widths and space structures: (i) FTIR spectra in the region of 4000–700 cm^{-1}. (ii) FT-IR spectra in the 3800–2600 cm^{-1} region.

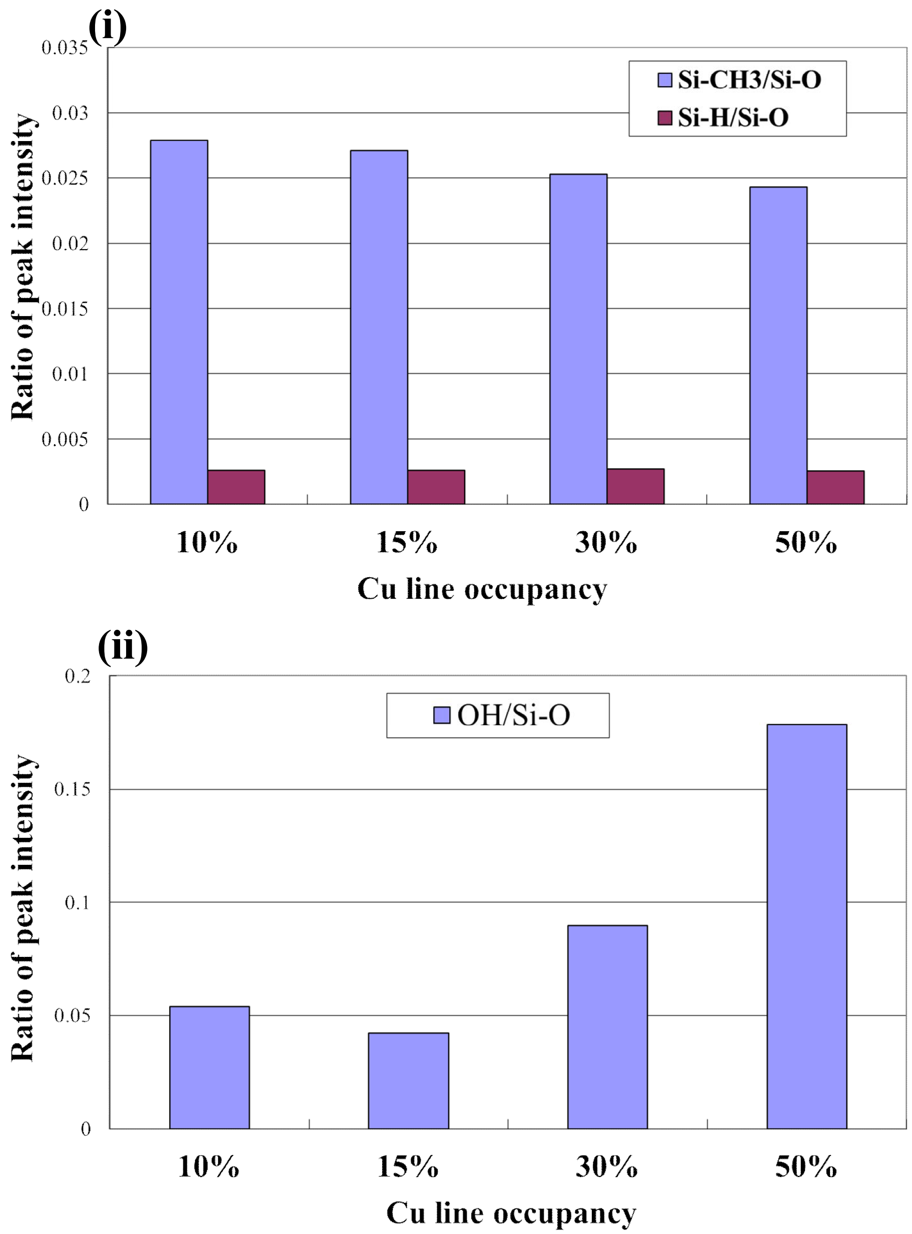

Fig. 3-7 Ratio of FT-IR peaks intensities: (i) Si-CH_3 and Si-H, (ii) OH.

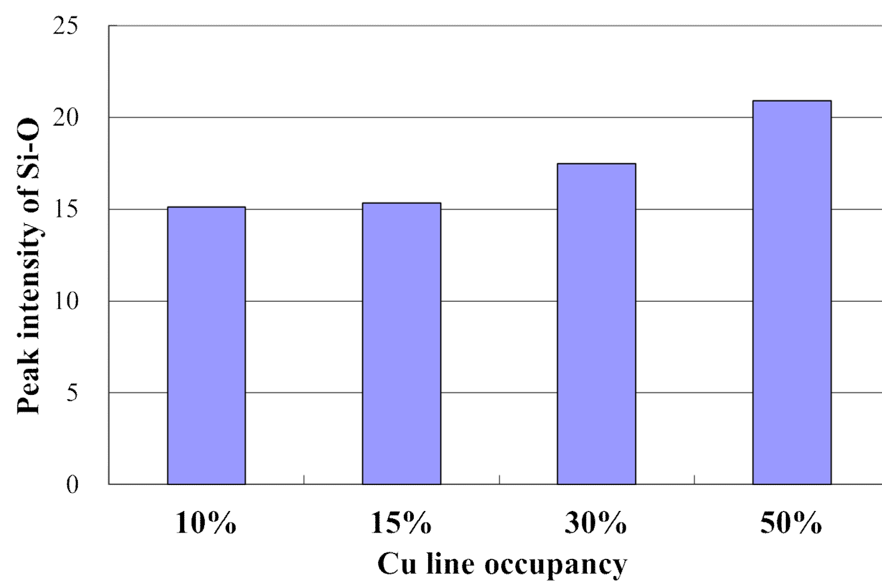

Fig. 3-8 FT-IR peaks intensities of Si-O stretching mode (I1050)

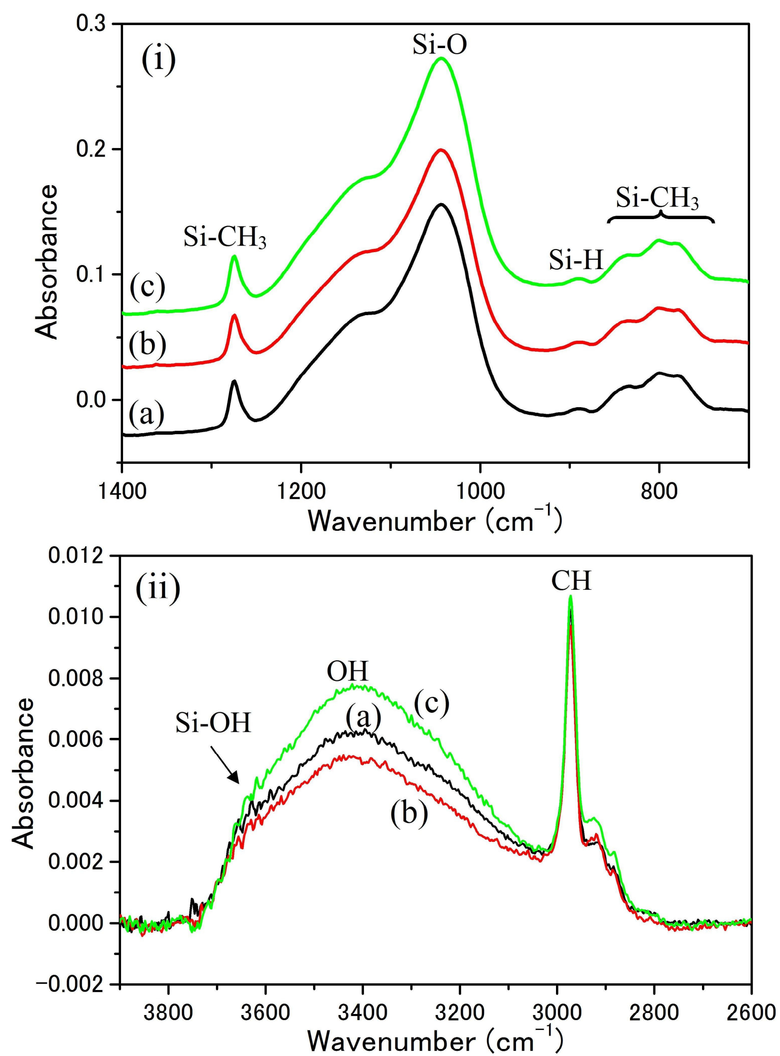

Fig. 3-9 FT-IR spectra for Cu/Low-k samples with different Cu line heights: (a) standard (b) short (c) long (L/S = 70 nm/70 nm). (i) in the 1400–700 cm^{-1} region and (ii) in the 3900–2600 cm^{-1} region.

(i)

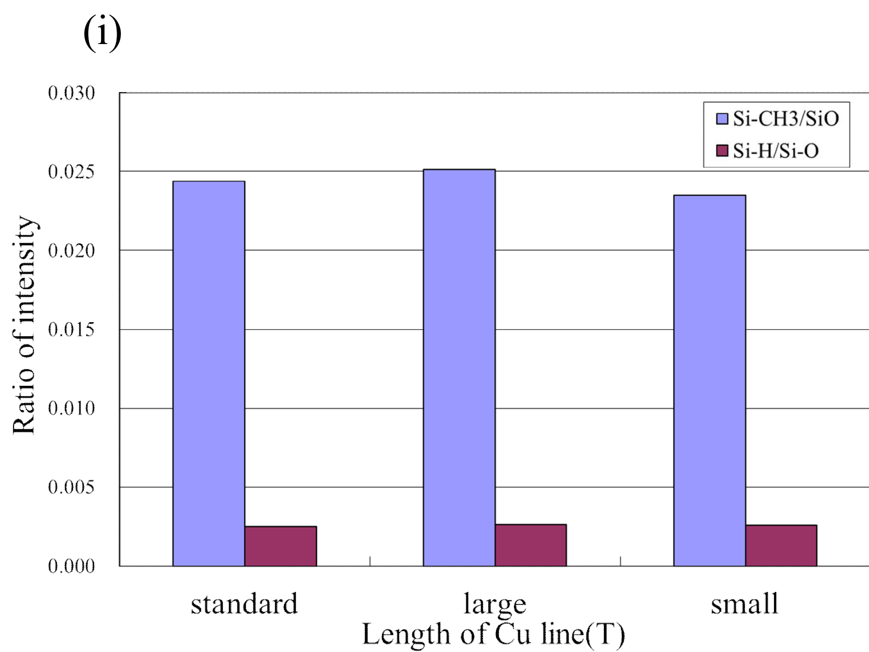

(ii)

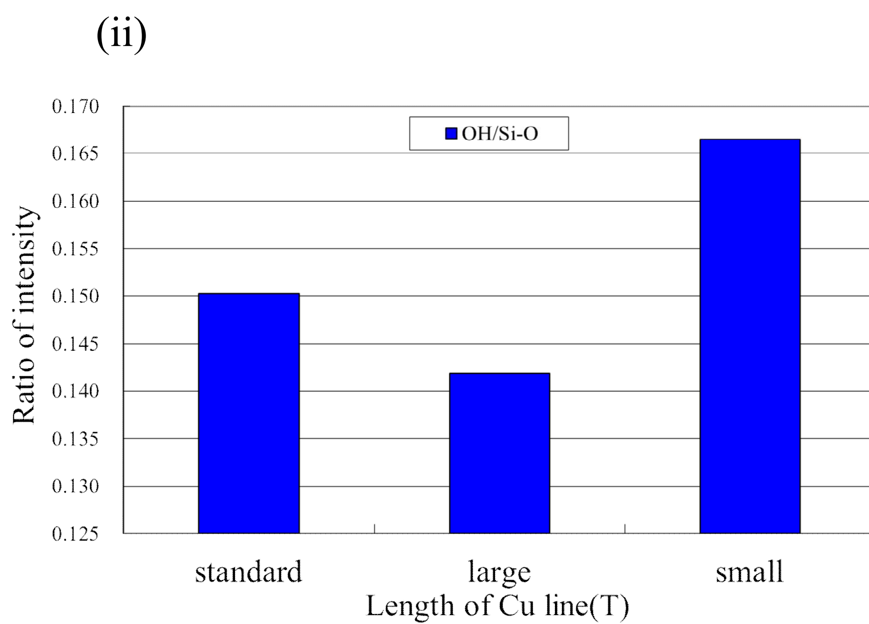

Fig. 3-10 Ratio of FT-IR peak intensities: (i) Si-CH_3 and Si-H, and (ii) OH.

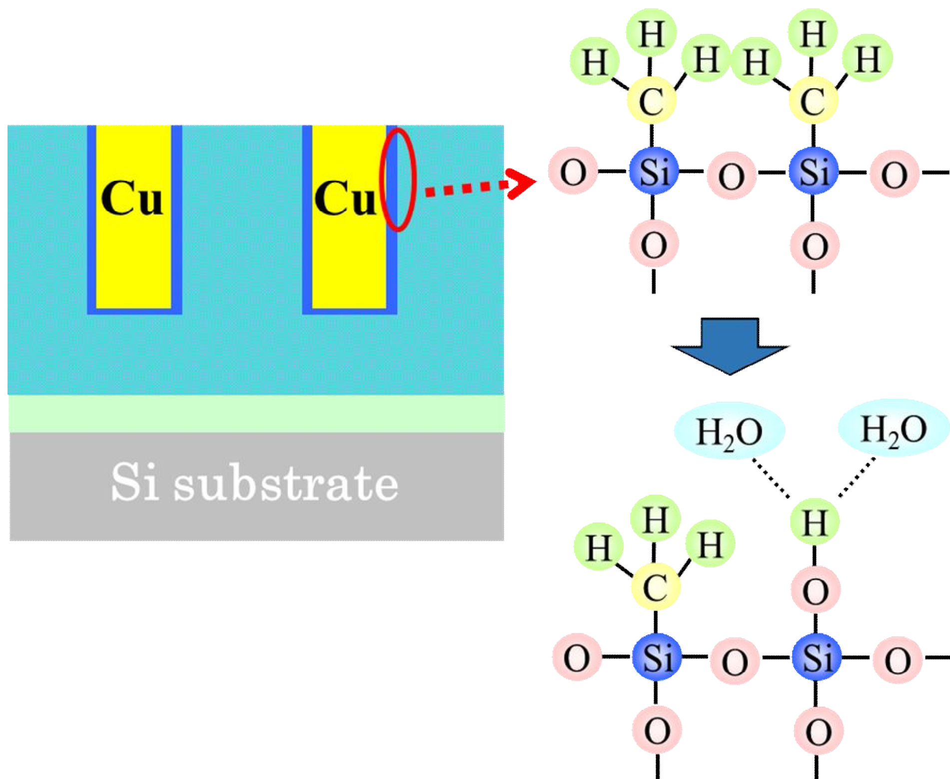

Fig. 3-11 Schematic view of the structural change in the sidewalls of the low-k film.

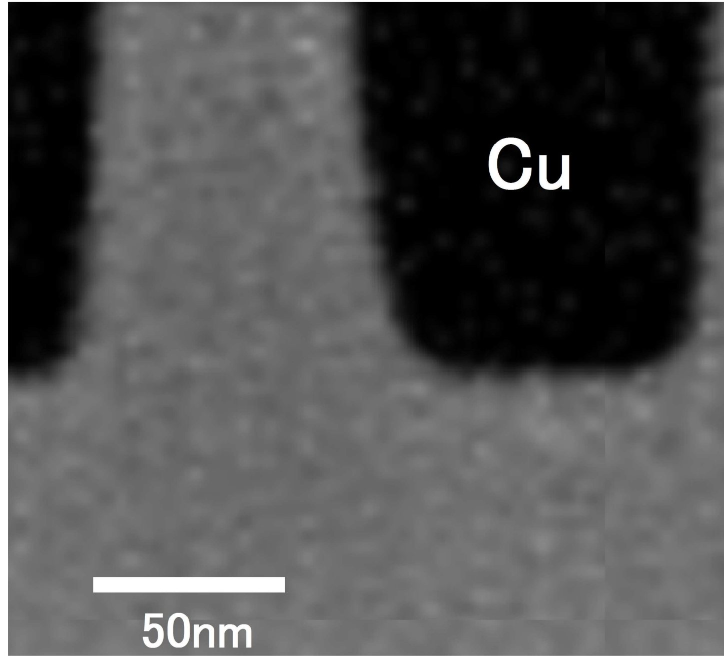

Fig. 3-12 Carbon composition mapping in low-k film by TEM-EELS.

Chapter 3

Characterization of Inhomogeneity in SiO_2 Films on 4H-SiC Epitaxial Substrate by a Combination of Fourier Transform Infrared and Cathodoluminescence Spectroscopy

ABSTRACT

We measured the Fourier transform infrared (FT-IR) and cathodoluminescence (CL) spectra of SiO_2 films grown on 4H-SiC substrates and confirmed that the phonon observed at around 1150–1250 cm^{-1} originates from the upper branch of the surface phonon polaritons (SPPs) in the SiO_2 films and that its frequency is sensitive to the oxide thickness. The relative intensity of the upper branch of SPPs normalized by that of the transverse optical phonon (TO) tended to increase with decreasing channel mobility (CM). A comparison between the FT-IR and CL measurements shows that the relative intensity is correlated with an inhomogeneity in the SiO_2/SiC interface, and the CM of SiC devices. A combination of FT-IR and CL spectroscopy provides us with a large amount of data on the inhomogeneity, defect, and oxide thickness of SiO_2 films on 4H-SiC substrates.

INTRODUCTION

Silicon carbide (SiC) is a well-known wide-bandgap semiconductor for high-power, high-frequency metal–oxide–semiconductor (MOS) device applications. The high interface trap densities (D_{it}) at the SiO_2/SiC interface and the high effective fixed charge densities (Q_{eff}), which are one to two orders of magnitude higher than those typically found at the SiO_2/Si interface (of the order of 10^{11} cm^{-2}),[1] degrade the channel mobility (CM).[2–5] The presence of interface traps in SiC MOS field-effect transistors (FETs) is attributed to (i) excess carbon,[4,6] (ii) interface defects due to the presence of threefold coordinated O and C interstitial atoms,[4,6] and (iii) point defects such as Si and O vacancies that extend into the SiC layer underneath the SiO_2/SiC interface.[7,8] H_2,[2] NO,[9,10] or N_2O[3,11–13] post-oxidation annealing (POA) effectively increases.

Fourier transform infrared (FT-IR) spectroscopy is an effective tool for investigating chemical bonding structures in thin oxide films. However, we cannot measure the transparent FT-IR spectra of SiO_2 films prepared on commercially available 4H-SiC substrates because of the strong absorptions due to the free carriers in the substrates. As a result, the attenuated total reflection (ATR) configuration is used as a highly sensitive method for investigating the SiO_2 films.[14] Transverse optical (TO) and longitudinal optical (LO) phonons in thermally grown SiO_2 films on a Si wafer have been observed at around 1072 and 1257 cm^{-1}, respectively.[8] These phonons are associated with the asymmetrical stretching of O in the intertetrahedral Si-O-Si bridge.[9] Although many studies have reported FT-IR spectroscopy of thermally grown SiO_2 films on Si wafers, none have focused on the microstructures in the interface between SiO_2 films and SiC wafers.[10,11]

Figure 4-1 shows the normal and grazing incidence and ATR spectra of a thick (100 nm) SiO_2 film on a bulk epitaxial 4H–SiC substrate[15]. We reported abnormal behavior of LO

phonon in a SiO_2 film on a 4H–SiC bulk epitaxial substrate. The peak frequency of the LO like phonon with an asymmetric line shape in the ATR spectrum was observed at around 1165 cm^{-1} and redshifted by approximately 92 cm^{-1} relative to that at the grazing incidence (40°) We assigned that the asymmetric modes located between 1110 and 1250 cm^{-1} were due to the upper and lower branches of surface polaritons (SPPs). [15] Furthermore, we divided the asymmetric modes located between 1110 and 1250 cm^{-1} into the two peaks with Lorentzian line shapes, and suggested that the two peaks divided were assigned to the upper and lower branches of SPPs at the air-SiO_2, and SiO_2-4H-SiC interfaces, respectively.[15]

In cathodoluminescence (CL) spectroscopy, luminescence of a sample subjected to electron beam irradiation is observed.[16-18] CL spectroscopy provides considerable information on defects in thin SiO_2 films. We prepared SiO_2 films (41-47 nm thick) grown on 4H-SiC (0001) Si, (1-100) M, and (11-20) A faces by POA in NO ambient at 1250 °C and found that the SiO_2 film grown on the 4H-SiC (11-20) A face had very large CM of 112 cm^2/Vs[18]. To clarify the origin of this high CM, we studied the changes in the CL spectra of SiO_2 films grown on 4H-SiC (0001) Si, (1-100) M, and (11-20) A faces subject to POA in NO ambient. For an acceleration voltage of 5 kV, the CL peak assigned to oxygen vacancy centers (OVCs) weakens by POA, whereas the CL peak related to Si-N bonding structures intensifies with increasing CM. This suggests that OVCs in the SiO_2/SiC interface are terminated by N. We have showed that NO ambient POA increases the CM more effectively than that by N_2O ambient.

We measured the FT-IR and CL spectra of SiO_2 films grown on 4H-SiC substrates. We found that the peak frequency of the upper branch of the SPPs in the SiO_2 films is sensitive to the oxide thickness and that the relative intensity of the upper branch of SPPs normalized by that of TO phonon increases with decreasing CM. Furthermore, for acceleration voltages of 3 and 5 kV, the CL peak around 600 nm, related to Si-N bonding

structures, becomes intense by POA in NO ambient at 1250°C. These results suggest that the interface trap densities (D_{it}) decrease and the CM in n-type MOS capacitors increases by the termination of dangling bonds by the N atom in the SiO_2/SiC interface. In this work, we reports that the relative intensity of the upper branch of SPPs normalized by that of the TO phonon is correlated with an inhomogeneity in the SiO_2/SiC interface in SiO_2 films and the CM in n-type MOS capacitors. A combination of FT-IR and CL spectroscopy provides us with a large amount of data on the inhomogeneity, defect, and oxide thickness of SiO_2 films on 4H-SiC substrates.

EXPERIMENTAL DETAIL

We prepared two sets of SiO_2 films, which were thermally grown on commercial epitaxial 4H-SiC and on bulk epitaxial 4H-SiC substrates in order to measure the transparent FT-IR spectra of SiO_2 films on 4H-SiC substrates. First, commercially available epitaxial layers (approximately 100 μm thick) on a 4° off-axis 4H-SiC (0001) Si face substrate were thermally oxidized in dry O_2 at 1150°C and then annealed in Ar ambient at 1300°C (we call those samples No.1-No.5, respectively). We measured a transparent FT-IR spectrum of No.5 in order to assign the optical phonons observed[15]. The oxide thickness was measured using ellipsometry. The oxide thickness was approximately 100 nm. Free-standing SiO_2 films (100 nm thick) on the bulk epitaxial substrate (approximately 100 μm thick) were obtained by removing them from the 4° off-axis 4H-SiC (0001).

Secondly, epitaxial layers (approximately 5 μm thick) were grown by chemical vapor deposition (CVD) on 4H-SiC 4° off-axis (0001) Si, (1-100) M, and (11-20) A faces (we call those samples Si, M, and A , respectively).[18] After these layers were RCA cleaned, they were thermally oxidized in dry O_2 at 1250 °C and then underwent POA in NO ambient at 1250 °C, followed by annealing in Ar ambient at 1250 °C. For the CL measurement, samples Si, M, and A (41-47 nm thick) were thinned using a dilute HF (0.05% HF) solution to a final thickness of 5 nm on the epitaxial 4H-SiC substrate (approximately 5 μm thick). The D_{it} values were estimated from high- (1 MHz) and low-frequency (quasi-static) capacitance–voltage (C–V) curves of n-type MOS capacitors, and the Q_{eff} values were determined from the flatband voltage in the C–V curves.[3] The voltage sweep rate was 0.1 V/s. The thicknesses, oxidation conditions, D_{it}, Q_{eff}, and CM values of the samples are listed in Table 4-I. The D_{it}, Q_{eff}, and CM values are within an error of ±5%.

FT-IR spectra were measured by a single-reflection ATR attachment in a Fourier transform

spectrometer (Varian FTS-55a). The incident light is p-polarized. The FT-IR measurements of each film were repeated 2 or 3 times and reproducible spectra were obtained. The accuracy of the peak frequency was within ±1 cm^{-1}.[15] We used a scanning electron microscope (SEM) with a Schottky-emission-type gun (HITACHI S-4300SE) as the excitation source for the CL measurements.[16-18] We repeated the CL measurements of each film three times and obtained reproducible CL spectra.

RESULTS AND DISCUSSION

Figures 4-2(a) and (b) shows the FT-IR spectra measured by the ATR configuration of a thick (100 nm) and thin (41-47 nm) SiO_2 films on 4H-SiC substrates, respectively. The TO and LO-like phonons were observed at around 1072 and 1200 cm^{-1}, respectively. The TO mode is associated with the asymmetrical stretching of O in the intertetrahedral Si-O-Si bridge. Surprisingly, the peak frequency of SPPs in the SiO_2 films was at the maximum redshifted by approximately of 30 to 90 cm^{-1} relative to that (1257 cm^{-1}) in thermally grown SiO_2 films on a Si substrate. As seen in Figs. 4-2(a) and (b), because the peak frequency of the TO phonon in the ATR spectrum agreed well with that at that in typical SiO_2 films on a Si wafer, the largest redshift 30 to 90 cm^{-1} relative to that (1257 cm^{-1}) in thermally grown SiO_2 films on a Si substrate cannot be explained by any of the factors such as the electromagnetic phase shift, inhomogeneity, densification, porosity, and SiO_2 film thickness. We indicated that the asymmetric modes located between 1110 and 1250 cm^{-1} are assigned to the upper and lower branches of SPPs[15], based on the model presented by Mills and Maradudin. [19]

For a comparison, We measured the ATR spectra of a standard SiO_2 film (approximately 50 nm thick) on a Si wafer thinned using dilute HF (0.05% HF) solution to a final thickness of 5 nm. Figure 4-3 shows the ATR spectra of a standard SiO_2 film on a Si wafer thinned using dilute HF (0.05% HF) solution to a final thickness of 5 nm. The peak frequency of the LO-like phonon shifts to a higher frequency, from 1150 cm^{-1} to 1250 cm^{-1}, with decreasing oxide thickness. Because the peak frequency of the TO phonon is independent of the oxide thickness, the large blueshift of the LO-like phonon observed for the standard SiO_2 film on the Si wafer also cannot be explained by any of the five factors as previously mentioned. The ATR spectra in Fig. 4-3 agree well with those in Fig. 4-2. In this work, we found that SPPs were also observed in the ATR spectra of a standard SiO_2 film on a Si wafer. Actually, Chen

et al. have observed an air-Si SPP at about 1142 cm^{-1} (8.76 μm) in a 1 μm thick SiO_2 film on a Si wafer and yielded a propagation length of about 11 μm for the silicon dioxide SPP resonance at about 1142 cm^{-1}. Their work[20] supports our observation[15] of SPPs in the SiO_2 films on 4H-SiC substrates.

We measured the ATR spectra of the SiO_2 film (No.5) on a bulk epitaxical 4H-SiC substrate thinned using dilute HF (0.05% HF) solution to a final thickness of 10 nm and found the peak frequency of the LO-like phonon shifts to a higher frequency, from 1165 cm^{-1} to 1250 cm^{-1}, with decreasing oxide thickness. [15] Figure 4-4 show the peak frequency dependence of the upper branch of SPPs on the oxide thickness for sample No.5. The peak frequencies for samples No.1-No.5 before the dilute HF treatment are also plotted in Fig. 4-4. As seen in Fig. 4-4, the peak frequency of the upper branch of SPPs shows an approximately linear shift with the oxide thickness. This suggests that the frequency of the upper branch of SPPs is sensitive to the oxide thickness. These two surface polaritons are considered to couple each other as the film thickness decreases. As a result, the upper branch shifts to a low-frequency side and the lower branch shifts to a high-frequency side. However, the surface polaritons seem to shift to a higher frequency, from 1165 cm^{-1} to 1250 cm^{-1}, with a decrease in the oxide thickness, although the peak frequency of the TO phonon is independent of the oxide thickness. The large blue shift observed in Fig. 4-3 with decreasing oxide thickness cannot be explained by a coupling between the two SPPs because the strong coupling between the two SPPs is considered to give rise to the red shift in the SPPs in Fig. 4-4. In the case of a very thin oxide thickness (10 nm), we speculate that ATR occurs between the Ge prism and the 4H-SiC substrate, and that the LO phonon by the electromagnetic wave evanescent from the Ge prism is mainly observed in a very thin SiO_2 film.

Figures 4-5(a) and (b) shows the relationship between the relative intensity of the upper

branch of SPPs normalized by that of TO phonon and the CM for samples No.1-No.5, Si, M, and A, respectively. As seen in Fig. 4-5, the relative intensity intends to increase with decreasing the CM. We could not observe SPPs in s-polarized configuration. Furthermore, SPPs are considered to become more intense with increasing an inhomogeneity of the films because of a breakdown in the conservation of momentum between the incident photon and phonon.[21] From this SPP characteristics, it is suggested that the inhomogeneity of SiO_2 films decreases in sample Nos.2 and 3 in Fig. 4-5 (a), and in the order of sample Si > M > A in Fig. 4-4 (b).

We previously measured CL spectra of the SiO_2 films (No.1-No.5) on epitaxial layers (approximately 5 μm thick), which were oxidized on the same deposition condition, at acceleration voltages of 3 and 5 kV. [17] We found that for an acceleration voltage of 5kV, CL peaks at 460 and 490 nm, assigned to oxygen vacancy centers (OVCs), become weak by POA in N_2O ambient at 1300°C whereas the CL peak around 580 nm, related to Si-N bonding structures, becomes intense. Furthermore, the peak assigned to N-Si_3 configurations in X-ray photoelectron spectroscopy spectra was observed in the SiO_2/SiC interface in only samples annealed in N_2O ambient. These results suggested that the D_{it} decrease and the CM in n-type MOS capacitors increases by the termination of dangling bonds by the N atom in the SiO_2/SiC interface. Based on this result and SPP characteristic, it is suggested that an increase of the CM in Fig.4-5(a) is caused by a decrease in the inhomogeneity in the SiO_2 films.

Figures 4-6 shows the CL spectra of SiO_2 films (samples Si, M, and A) thinned using a dilute HF (0.05% HF) solution to a final thickness of 5 nm on the epitaxial 4H-SiC substrates (approximately 5 μm thick) and measured at acceleration voltages of 3 kV (Fig. 4-6(a)) and 5 kV (Fig.4-6(b)). The CL peak at 390 nm originates from a bound exciton. The CL peak at 540 nm is assigned to donor-acceptor pairs[17] or defect-related emission bands. [22-23] CL peaks

were observed at 460, 490, 600, and around 640-670 nm for the SiO_2 films on the 4H-SiC substrates. The CL peaks at 460 and 490 nm were attributed to OVCs, whereas the CL peaks at 600 nm and around 640-670 nm were attributed to Si-N bonding structures and non-bridging oxidation hole centers (NBOHCs), respectively.[16-18] The weak CL peak at around 280 nm is considered to originate from OVCs.[18] The broad CL spectra of the SiO_2 films were for convenience of quantitative analysis decomposed into six CL peaks with Gaussian line shapes and the obtained results did not depend on whether the line shape was Lorentzian or Gaussian. [18] As shown in Figs. 4-6, the CL peak around 600 nm tends to increase in strength in the order sample Si < M < A when measured at acceleration voltages of both 3 and 5 kV.

Figures 4-7 shows the relationship between the CM of the SiC-MOSFET and the relative CL intensity at 600 nm, normalized by that around 670 nm, measured at acceleration voltages of 3kV (Fig. 6(a)) and 5 kV(Fig. 6(b)). As shown in Fig. 4-7, the relative intensity increases in strength in the order of sample Si < M < A at 3 and 5 kV. This result shows that the POA decreased the number of NBOHCs by N termination in the SiO_2/SiC interface in the order of samples Si > M > A, and that the inhomogeneity of SiO_2 films decreases in the order of samples Si > M > A, resulting in an increase of the CM.

In Fig.4-5(b), We found that the relative intensity of the upper branch of the SPPs normalized by that of the TO phonon increases with decreasing CM. Based upon a comparison between Figs. 4-5(b) and 4-7, we concluded that the SPP intensity is correlated with an inhomogeneity of the SiO_2 films, and that it can be useful for a monitor of the inhomogeneity in the SiO_2/SiC interface and the CM. A combination of FT-IR and CL spectroscopy provides us with a large amount of data on the inhomogeneity, defect and oxide thickness of SiO_2 films on 4H-SiC substrates.

As we can see in Figs. 4-2 and 4-5, the absolute relative intensity of the upper branch

of the SPPs normalized by that of the TO phonon depends on whether the SiO_2 films are undergone by POA in N_2O or NO ambient. As seen in Table 4-I, samples No.1-No.5 are thermally oxidized at 1150°C whereas samples Si, M, and A are oxidized at 1250°C. This difference of the absolute relative intensity among the samples cannot be explained by the difference of the oxide thickness[16]. We believe that the difference of the absolute intensity between Figs.4-2(a) and (b) is caused by the difference of the thermal oxidation temperature.

CONCLUSION

We measured the FT-IR and CL spectra of SiO_2 films grown on 4H-SiC substrates and confirmed that the phonon observed at around 1150–1250 cm^{-1} originates from the upper branch of the surface phonon polaritons (SPPs) in the SiO_2 films and that its frequency is sensitive to the oxide thickness. The relative intensity of the upper branch of SPPs normalized by that of the transverse optical (TO) phonon tended to increase with decreasing channel mobility (CM). Furthermore, for acceleration voltages of both acceleration voltages 3 and 5 kV, the CL peak around 600 nm, related to Si-N bonding structures, becomes intense by post-oxidation annealing (POA) in NO ambient at 1250°C. These results suggest that the interface trap densities (D_{it}) decrease and the CM in n-type MOS capacitors increases by the termination of dangling bonds by the N atom in the SiO_2/SiC interface. From a comparison of the FT-IR and CL measurements, the SPP intensity is considered to be correlated with the inhomogeneity of the SiO_2 films, and with the CM in n-type MOS capacitors. A combination of FT-IR and CL spectroscopy provides us with a large amount of data on the inhomogeneity, defect and oxide thickness of SiO_2 films on 4H-SiC substrates.

REFERENCES

[1]S. M. Sze, "MOSFET and Related Devices". In: S.M.Sze, editor. Semiconductor Devices: Physics and Technology . New York: John Wiley & Sons, pp. 169(2002).

[2]R K. Fukuda, M. Kato, K. Kojima, and J. Senzaki, Appl. Phys. Lett. 84, 2088 (2004).

[3]T. Kimoto, Y. Kanzaki, M. Noborio, H. Kawano, and H. Matsunami, Jpn. J. Appl. Phys. 44, 1213 (2005).

[4]V. V. Afanasev, M. Bassler, G. Pensl, and M. Schulz, Phys. Stat. Sol. (a). 162(1), 321 (1997).

[5]J. A. Cooper, Jr. Phys. Stat. Sol. (a). 162(1), 305 (1997).

[6]T. Zheleva, A. Lelis, G. Duscher, F. Liu, I. Levin, and M. Das, Appl. Phys. Lett. 93, 022108 (2008).

[7]T. Y. Luo, M. Laughery, G. A. Brown, H. N. Al-Shareef, V. H. C Watt, A. Karamcheti, M. D. Jackson and H. R. Huff , Electron Device Letters. 21, 382 (2000).

[8]N. Nagai, K. Terada, Y. Muraji, H. Hashimoto, T. Maeda, Y. Maeda, E. Tahara, N. Tokai, and A. Hatta, J. Appl. Phys. 91, 4747 (2002).

[9]H. J. von Bardeleben, J. L. Cantin, I. C. Vickridge, Y. Song, S. Dhar, L. C. Feldman, J. R. Williams, L. Ke,Y. Shishkin, R. P. Devaty, and W. J. Choyke : Mater. Sci. Forum. 483-485, 277 (2005).

[10]P. Jamet, S. Dimitrijev, and P. Tanner, J. Appl. Phys. 90, 5058 (2001).

[11] L. A. Lipkin, M. K. Das, and J. W. Palmour: Mat. Sci. Forum: 389-393, 985 (2002).

[12]Y. Kanzaki, H. Kinbara, H. Kosugi, J. Suda, T. Kimoto and H. Matsunami: Mater. Sci. Forum. 457-460, 1429 (2004).

[13] M. K. Das, Mater. Sci. Forum. 457-460, 1275 (2004).

[14]M. Yoshikawa and N. Nagai, In: J. M. Chalmers and P. R. Griffiths, editors. Handbook of Vibrational Spectroscopy. Chichester, UK: Wiley, 2002, Pp. 2593.

[15] M. Yoshikawa, H. Seki, T. Yamane,Y. Nanen, M. Kato, and T. Kimoto, Appl.Spectrosc. 67, 542 (2013).

[16]M. Yoshikawa, H. Seki, K. Inoue, K. Matsuda, Y. Tanahashi, H. Sako,Y. Nanen, M. Kato, and T. Kimoto, Appl. Spectrosc. 65, 543 (2011).

[17]M.Yoshikawa, S.Ogawa, K. Inoue, H. Seki, Y.Tanahashi, H.Sako,Y. Nanen, M. Kato, and T. Kimoto, Appl. Phys. Lett. 100, 082105 (2012).

[18]M.Yoshikawa, K. Inoue, H. Seki, Y. Nanen, M. Kato, and T. Kimoto, Appl. Phys. Lett. 102, 051612 (2013).

[19]D. L. Mills and A. A. Maradudin, Phys. Rev. Lett. 31, 372 (1973).

[20]D.A.Chen and G.Chen, Appl. Phys. Lett. 91, 121906 (2007).

[21] S. Ushioda, A. Aziza, J. B.Valdez and G. Mattei, Phys. Rev. B. 19, 4012 (1979).

[22]S. G. Sridhara et al, J. Appl. Phys. 83, 7909 (1998).

[23]A. Kakanakova-Georgieva, R. Yakimova, and A. Henry, J. Appl. Phys. 91, 2890 (2002).

Table. 4-I. Thickness, oxidation condition, D_{it}, Q_{eff}, and CM of thermally grown SiO_2 films on the 4H-SiC substrates.

Face	Thickness (nm)[a]	Thermal oxidation condition	Post-oxidation annealing condition	D_{it} $(cm^2eV)^{-1}$ $(E_c - 0.2eV)$[b]	Q_{eff} (cm^{-2})	Mobility (cm^2/Vs)
Si No.1	100	1150 °C 12h	N_2O anneal : - Ar anneal : -	5.0×10^{12}	-1.5×10^{12}	4±1
Si No.2	100	1150 °C 12h	N_2O anneal 1300 °C, 2h Ar anneal 1300 °C, 0.5h	5.0×10^{11}	-2.3×10^{11}	24±1
Si No.3	100	1150 °C 12h	N_2O anneal 1300 °C, 2h Ar anneal 1300 °C, 5h	4.0×10^{11}	-2.8×10^{11}	34±1
Si No.4	100	1150 °C 12h	N_2O anneal : - Ar anneal 1300 °C, 0.5h	1.0×10^{12}	2.6×10^{11}	5±1
Si No.5	100	1150 °C 12h	N_2O anneal : - Ar anneal 1300 °C, 5h	1.0×10^{12}	3.9×10^{11}	7±1
Si	41(5)	1250 °C 60 min	NO anneal 1250 °C, 60 min Ar anneal 1250 °C, 60 min	5.0×10^{11}	1.5×10^{11}	35±1
A	47(5)	1250 °C 10 min	NO anneal 1250 °C, 60 min Ar anneal 1250 °C, 60 min	3.4×10^{11}	1.8×10^{11}	112±1
M	45(5)	1250 °C 10 min	NO anneal 1250 °C, 60 min Ar anneal 1250 °C, 60 min	3.6×10^{11}	1.7×10^{11}	105±1

[a] Values in parentheses are the thickness after thinning with HF solution.

[b] Ec, critical excitation energy

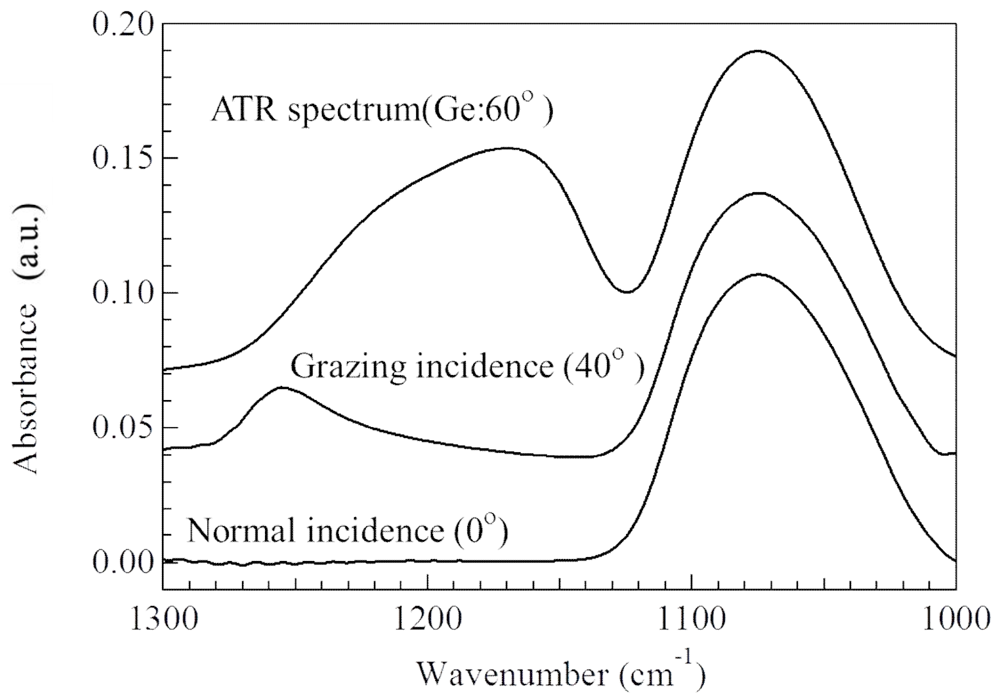

Fig. 4-1. Normal and grazing incidence and ATR spectra of thick (100 nm) SiO_2 film on bulk epitaxial 4H–SiC substrate. The incident angle in the ATR spectrum was fixed at 60°, and a Ge crystal was used as an internal reflection element (ATR prism).

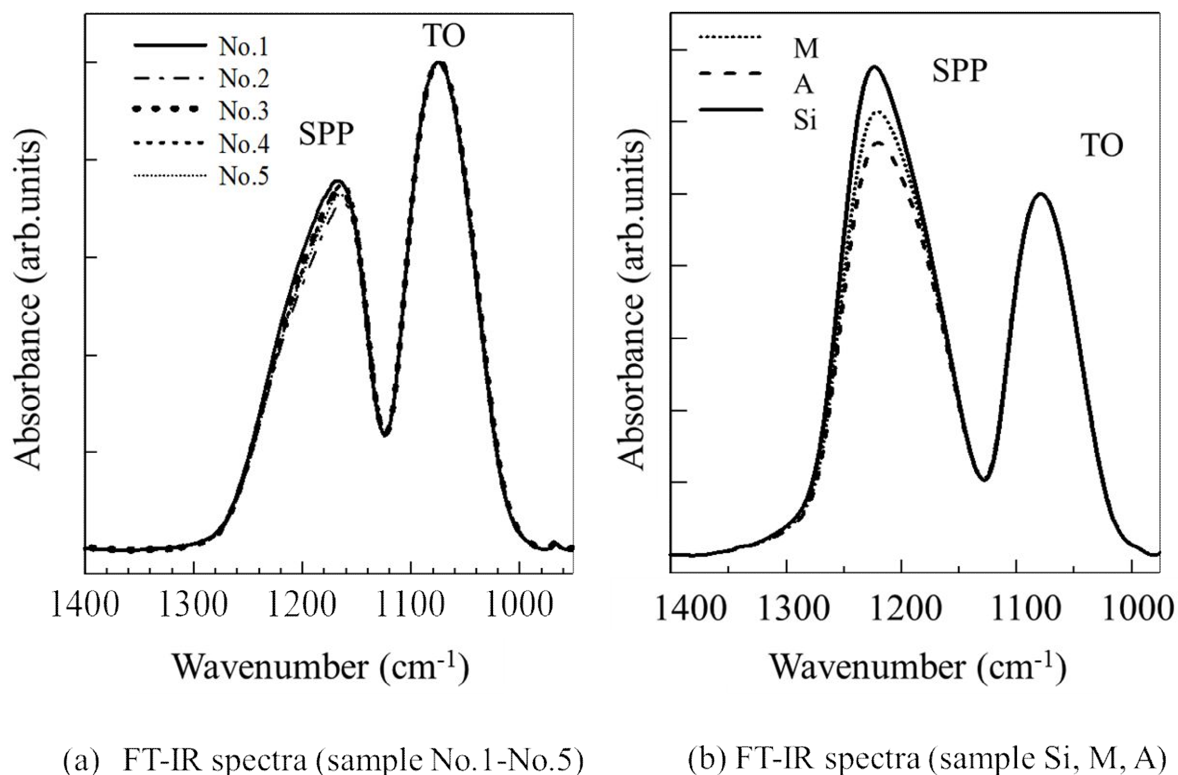

Fig. 4-2. FT-IR spectra measured using the ATR configuration of films before the dilute HF etching (a) thick (100 nm) SiO_2 films (sample No.1-No.5) on a bulk epitaxial 4H-SiC substrate, and (b) thin (41-47 nm) SiO_2 films (sample Si, M, A) on an epitaxial 4H-SiC substrate (approximately 5 μm thick).

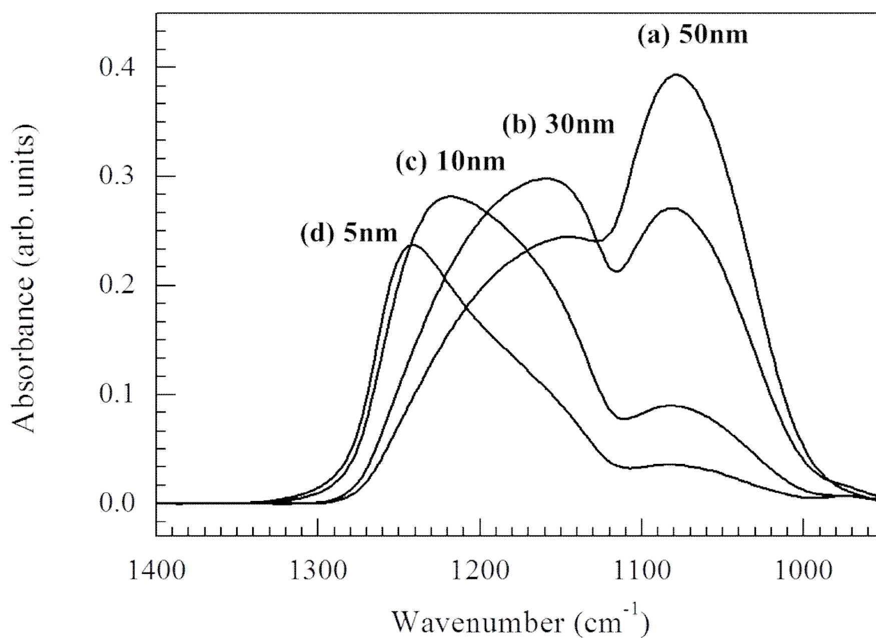

Fig. 4-3. ATR spectra of a standard SiO_2 film on a Si substrate thinned using dilute HF (0.05% HF) solution to final thickness of 5 nm: (a) Thickness of 50 nm, (b) Thickness of 30 nm, (c) Thickness of 10 nm, and (d) Thickness of 5 nm. The incident angle in the ATR spectra was fixed at 60° with a Ge crystal.

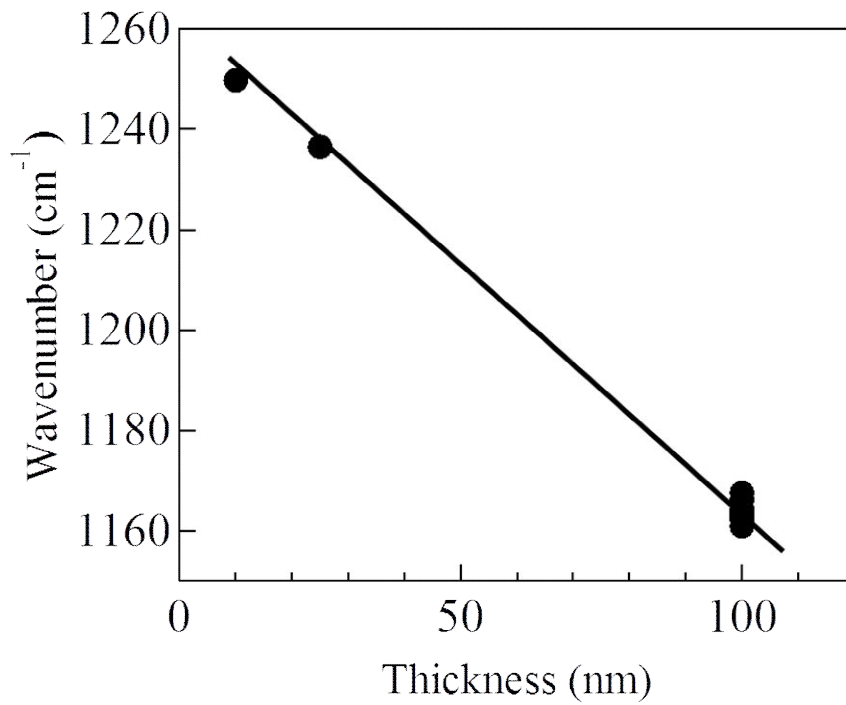

Fig. 4-4. Peak frequency dependence of the upper branch of SPPs on the oxide thickness for sample No. 5. The peak frequencies for samples No. 1-5 before the dilute HF treatment are also plotted.

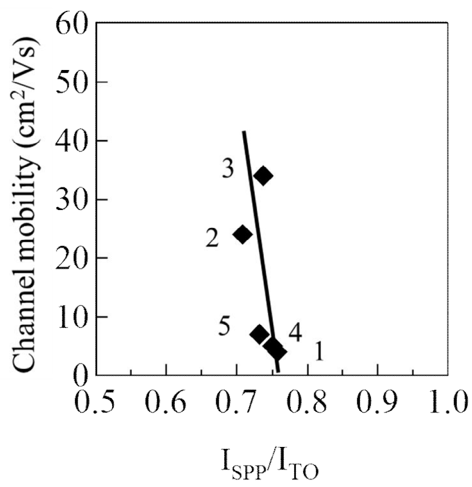

(a)

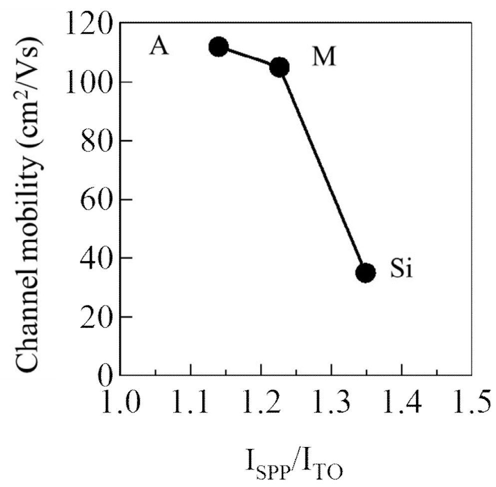

(b)

Fig. 4-5. Relationship between the relative intensity of the upper branch of SPPs normalized by that of TO phonon, and channel mobility (CM): (a) For samples No.1-No.5, (b) For samples Si, A and M.

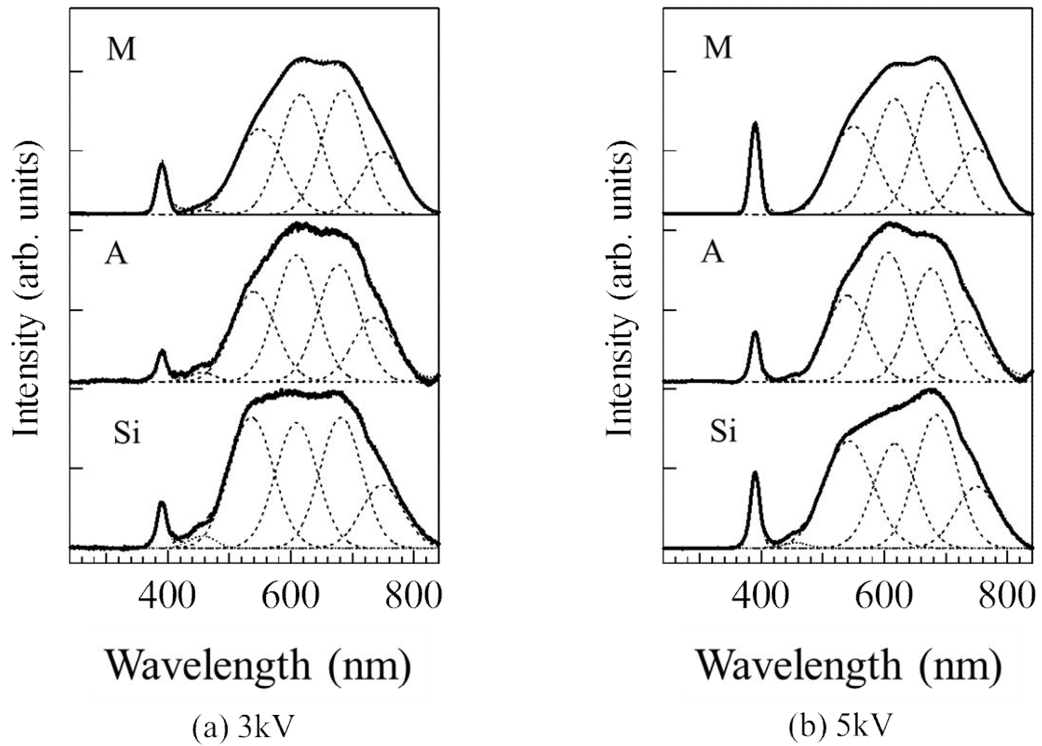

(a) 3kV

(b) 5kV

Fig. 4-6. CL spectra for samples Si, M, and A, SiO_2 films: (a) Measured at an acceleration voltage of 3 kV and (b) Measured at an acceleration voltage of 5 kV. The samples were thinned using a dilute HF (0.05% HF) solution to a final thickness of 5 nm on the epitaxial 4H-SiC substrate (approximately 5 μm thick).

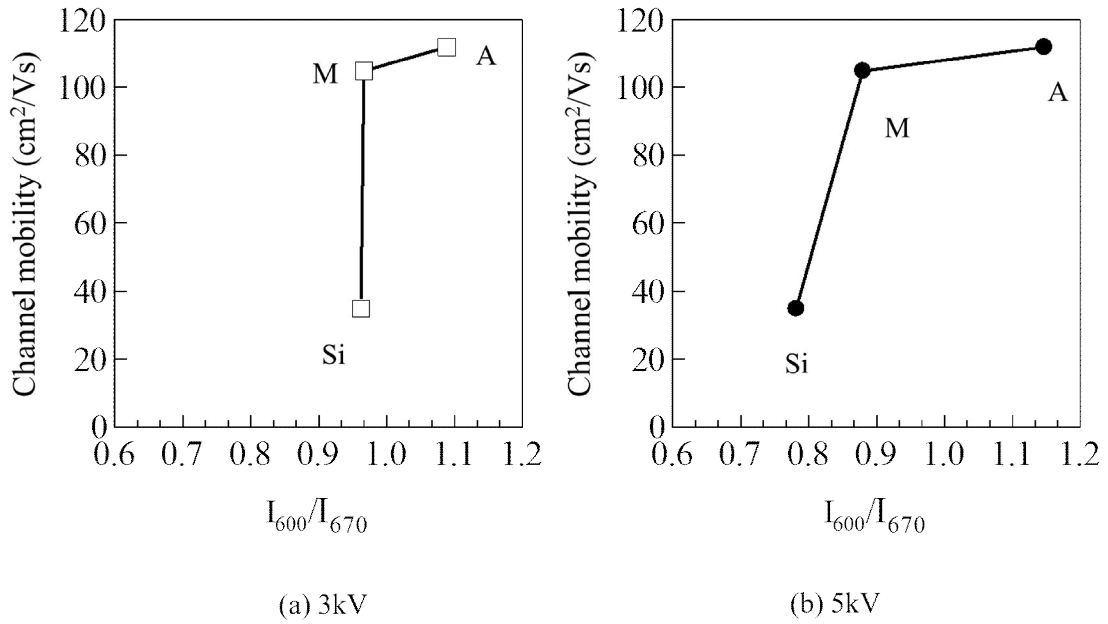

Fig. 4-7. Relationship between the CM of the SiC-MOSFET and the relative CL intensity at 600 nm, normalized by that at 670 nm. (a) Measured at an acceleration voltage of 3 kV and (b) Measured at an acceleration voltage of 5 kV.

Chapter 4

Characterization of Thermal Oxides on 4H-SiC Epitaxial Substrates Using Fourier-Transform Infrared Spectroscopy

ABSTRACT

Fourier transform infrared (FT-IR) spectra were measured for thermal oxides with different electrical properties grown on 4H-SiC substrates. The peak frequency of the transverse optical (TO) phonon mode was blue-shifted by 5 cm^{-1} as the oxide-layer thickness decreased to 3 nm. The blue shift of the TO mode indicates interfacial compressive stress in the oxide. Comparison of data for the oxide on a SiC substrate with that for similar oxides on a Si substrate implies that the peak shift of the TO mode at the SiO_2/SiC interface is larger than that of SiO_2/Si, which suggests that the interfacial stress for the oxide on the SiC substrate is larger than that on the Si substrate. For the SiO_2/SiC interfacial region (<3 nm oxide thickness), despite the fact that the blue shift of the TO modes becomes larger while approaching the oxide/SiC interface, the peak frequency of the TO modes red-shifts at the oxide/SiC interface. The peak-frequency shift of the TO mode for the sample without post-oxidation annealing was larger than that for the samples post-annealed in a nitric oxide atmosphere. The channel mobilities are correlated with the degree of shift of the TO mode when the oxide thickness is <3 nm. It appears that the compressive stress at the SiO_2/SiC interface generates silicon suboxide components and weakens the Si-O bonds. As the result, the TO mode was red-shifted and the oxygen deficiency increased to relax the compressive stress in the oxide with <3 nm thickness. FT-IR measurements provide unique and useful information about stress and inhomogeneity at the oxide /SiC interface.

.

INTRODUCTION

As discussed previously in Chapter 3, there are several longstanding problems in SiC technology concerning high values of trap densities (D_{it}) and high fixed-charge density (Q_{eff}) at the SiO_2/SiC interface, as such high values can degrade the channel mobility of SiC MOSFETs. Various studies have been carried out to improve these characteristics, with one promising method involving post-annealing treatment in different atmospheres such as H_2,[1] NO,[2-5] N_2O,[6,7] and $POCl_3$.[8]

FT-IR spectroscopy is a powerful analytical method for investigating chemical bonding structures in thin oxide films.[9-12] Many reports have already been published regarding FT-IR studies on the chemical bonding structure, properties, interfacial structures, and functions of thin films.[10-27] There are also a few prior reports on the use of FT-IR to characterize the chemical bonding structure of SiO_2 on SiC substrates.[28-31] Queeney *et al.*[11] studied the microscopic structure of SiO_2/Si interfaces using an IR transmittance technique for oxides with different thicknesses of less than 3 nm using a wet etching technique. Nagai *et al.*[12] also studied such interfacial structures using IR microspectroscopy and original etching pretreatment. These studies concluded that the amount of TO frequency shift at an oxide/Si interface is correlated with its electrical properties, such as leakage current and dielectric breakdown. Thus, these FT-IR studies provided valuable information about the present chemical bonding structures that was useful for improving the relevant manufacturing processes. The relationship between the state of a SiO_2/SiC interface and its electrical properties has been previously reported.[32-35] However, the use of FT-IR for this purpose has not yet been reported. In Chapter 4, we have investigated the chemical bonding structures at oxide/SiC interfaces by FT-IR measurements, and determined the relationship between the chemical bonding state of an oxide/SiC interface and its electrical properties. FT-IR-ATR

spectra were collected from thermal oxides in oxide/SiC interfaces that were subjected to post-oxidation annealing (POA) in a nitric oxide (NO) atmosphere. The samples that were selected for ATR measurements featured different electrical properties, such as interface state density. We have also discussed the chemical bonding structure at the oxide/SiC interface which affects these electrical properties, and the differences between oxides on SiC and Si substrates. The obtained results are useful to develop higher-quality oxides on SiC substrates and to accelerate SiC device development.

EXPERIMENTAL DETAIL

Epitaxial layers of N-doped (5×10^{15} cm^{-3}) 4H-SiC (~8 μm thick) were grown by chemical vapor deposition (CVD) on a 4° off-axis 4H-SiC (0001) Si face. After these layers were cleaned by the well-known RCA (Radio Corporation of America) process, they were thermally oxidized for 60 min in dry O_2 at 1300 °C. The oxide layer thickness was determined to be about 75 nm. Three types of samples were prepared in the present study, as listed in Table 5-I. The samples designated as "OX" did not receive any post-oxidation treatment; the samples designated as "NO" were subjected to POA in a nitric oxide atmosphere at 1250 °C for 30 min; and the samples designated as "NL" were subjected to the same POA for a longer time (180 min).

FT-IR spectra were measured using a single-reflection ATR attachment in a Fourier transform spectrometer (Bio-Rad FTS-55a) with an infrared polarizer to generate p- or s-polarized infrared light. Bands due to the vibrational modes that are perpendicular to the surface of the SiC substrate can be observed by using p-polarized light (p-pol), and those due to the vibrational modes that are parallel to the surface can be independently obtained by employing s-polarized light (s-pol). The incident angle was fixed at 60°, and a Ge crystal was used as an internal-reflection element. The air gaps between the Ge prism and the samples were not controlled. We used diluted hydrofluoric acid (HF) solution (1%) to etch the oxide. The ATR measurements were performed for non-etched samples and for various SiO_2 film thicknesses (all of which were less than 8 nm in thickness) by repeating the ATR measurements and wet etching. The thicknesses of the oxides were measured with a spectroscopic ellipsometer (J. A. Woollam Co. M-2000) and were calculated by using the fixed optical constant that was obtained for the non-treated samples. We also carried out transmittance IR measurements for thermal oxides on Si with different thicknesses of less

than 9 nm to compare the chemical bonding structures of oxides on the SiC and Si substrates.

Secondary ion mass spectrometry (SIMS) was used to estimate the amount of carbon and nitrogen impurities as a function of depth. The SIMS measurement was performed with a Magnetic-Sector type instrument (Cameca IMS-6f) to detect nitrogen at the interface between the oxide and the SiC substrates; a quadrupole type instrument (PHI ADEPT-1010) was used to measure the amount of carbon in the oxide.

Cathodoluminescence (CL) spectroscopy provides extensive information about defects in SiO_2 films.[36, 37] The CL spectra were recorded using a Jobin Yvon HR-320 single monochromator equipped with a 1024-channel charge-coupled-device (CCD) detector. The CL spectra were recorded at acceleration voltages of 3 kV and 5 kV at room temperature, with a beam current of less than 5 nA. The electron beam was focused with an incident beam diameter of less than 10 nm. To minimize the degradation caused by the electron beam irradiation, most CL spectra were measured for a period of 60 s.

RESULTS AND DISCUSSION

Figures 5-1(a) and (b) show FT-IR spectra of the non-etched samples measured using the ATR configuration with p-polarized [Fig. 5-1(a)] and s-polarized [Fig. 5-1(b)] light sources, respectively. The SiC substrate absorbs IR radiation in the same wavenumber region as the SiO_2,[28] but the spectra shown in the figure are difference spectra in which the IR absorption of the SiC substrate was already subtracted. The peaks due to the TO and LO modes were previously observed at around 1072 and 1190 cm^{-1}, respectively, for thermally grown thermal oxides on a Si wafer.[10-12,25,26] In Fig. 5-1(a), the broad phonon modes appear strongly in the 1180–1250 cm^{-1} region of the p-polarized spectrum, whereas they are barely visible under s-polarized illumination. However, the TO mode at ~1080 cm^{-1} is strongly observed in Fig. 5-1(a) and (b). Figure 5-2 shows the peak position of the LO and TO modes for the non-etched oxides. The peak frequency of the TO mode and LO mode for sample OX shifts to a higher wavenumber than that of samples ON and OL. Regarding the LO mode shift, we previously reported the appearance of broad bands in the region of 1250-1150 cm^{-1} in p-polarized light spectrum and their disappearance in s-polarized light spectrum; in that paper, we confirmed that the band originated from surface phonon polaritons (SPPs).[30] This mode is sensitive to interfacial structure. Thus, the difference of the frequency of the LO modes may reflect the difference in interfacial structures of these samples.

On the other hand, regarding the TO mode shift, we reported TO peak positions of samples with different oxide thicknesses on a SiC substrate.[38] The TO peak positions were blue-shifted by 10 cm^{-1} as the oxide thickness decreased from 130 nm to 8 nm. We concluded that this blue shift was caused by compressive stress at the interface between the thermal oxide and the SiC substrate due to different thermal expansions and elastic moduli between the thermal oxide and the SiC substrate.[38] Chokawa *et al*.[39] investigated the influence of

oxidation on the defect formation by first-principles calculations. They found that Si-C bonds around inserted O atoms are shortened by about 5%, indicating that the insertion of O atoms causes large compressive strain. It appears that the TO and LO blue shifts for Sample OX were caused by compressive stress at the oxide/SiC interface. Furthermore, we investigated the details of the interfacial structure by repeating the ATR measurements and wet etching.

Figures 5-3(a) and (b) show FT-IR-ATR spectra of SiO_2 grown on a 4H-SiC substrate (sample OX) with different thicknesses (all of which were less than 8 nm) measured by the ATR technique using p-polarized and s-polarized light, respectively, after etching the SiO_2 layers in 1% HF to reduce their thickness from the original value of 75 nm down to < 8 nm As seen in Fig. 5-3(a) and (b), the peak intensity of the LO and TO modes decreases gradually as the thickness decreases, and finally disappears; the rate of decrease is similar for the spectra measured by either type of polarized light, and we are able to obtain information about the oxide/SiC interfacial structure.

Figure 5-4(a) and (b) plot the LO and TO mode peak frequencies obtained from Fig. 5-2 as a function of the oxide layer thickness. It can be seen from Fig. 5-3(a) that for thick oxide with a thickness of 3–8 nm, the peak frequency of the LO mode is red-shifted as the thickness of the oxide layer decreases. Figure 5-4(b) reveals that the peak frequency of the TO mode is blue-shifted as the thickness of the oxide layer decreases down to 3 nm and then red-shifted as the oxide thickness decreases for SiO_2 thinner than 3 nm. The blue shift of sample OX is larger than that of samples NO and NL for thick oxide with a thickness of 3–8 nm. This indicates that the interfacial compressive stress for sample OX is larger than that for samples NO and NL. Hirai and Kita[28] measured the FT-IR spectra of thermally grown oxides on the Si and C faces of 4H-SiC and reported that the peak frequency of the TO modes was almost constant for the thicker oxides with a thickness of 5–30 nm; their result is different from our results. The difference of the TO mode frequency behavior might be caused by the different

oxidation temperatures or the quality of the SiC substrate.

The peak frequency of the TO modes is red-shifted as the oxide thickness decreases for SiO_2 thinner than 3 nm in Fig. 5-4(b). Despite the fact that the blue shift of the TO modes becomes larger while approaching the oxide/SiC interface, the peak frequency of the TO modes red-shifts at the oxide/SiC interface for all samples. The TO mode peak-frequency shift for sample OX is larger than that for samples NO and NL with a SiO_2 film thickness of less than 3 nm. These results indicate that the chemical bonding structures of sample OX change drastically at the oxide/Si interface region within 3 nm from the SiC surface, compared with samples NO and NL. These changes may be caused primarily by the compositional inhomogeneity, defects such as non-bridging oxidation hole centers, or the effects of forming the Si–N bond. Sample OX, which has the smallest channel mobility, exhibits the largest shift of TO peak frequency for the SiO_2/SiC structure in the oxide-thickness range smaller than 3 nm. The amount of TO shift at the oxide/SiC interface is defined as the difference between TO frequencies with oxide thickness from 3 nm to 0.5 nm in this study. Figure 5-5 shows the amount of shift in the TO mode with an oxide thickness of less than 3 nm vs. channel mobility. The channel mobilities are correlated with the amount of shift in the TO mode, and the amount of TO mode shift is larger when the channel mobility is lower. We have demonstrated for the first time that the TO frequency shift at the oxide/SiC interface is related to its electrical properties.

Figure 5-6(a) displays transmittance spectra of the thermal oxides with different thicknesses (all less than 9 nm) prepared by using the wet etching pretreatments reported in Ref.12. The transmittance measurements can be carried out for the oxides on Si substrates. We are able to compare the degree of the shift of the TO modes for SiO_2 on SiC substrates with those on Si substrates while the thickness of SiO_2 is varied. Figure 5-6(b) plots the peak frequency of the TO mode obtained from Fig. 5-6(a) versus the thickness of the oxide layer.

For the thick oxide with a thickness of 2–9 nm, the peak frequency of the TO modes is almost constant; however, for the oxide with thicknesses less than 2 nm, the peak frequency of the TO mode is red-shifted. Comparing these data, we have found that the peak frequency of the TO mode for the oxide on the SiC substrate is blue-shifted as the oxide thickness decreases; however, that for the Si substrate remains at almost the same wavenumber. It is very likely that the difference in the shift of the TO mode between the oxide on the SiC substrate and that on the Si substrate is caused by differences in the compressive stress at the interface due to different thermal expansion and elastic moduli between the SiC and Si substrates. By comparing the data for the oxide on the SiC substrate with that for similar oxide on the Si substrate, it appears that the interfacial stress for the oxide on the SiC substrate is larger than that on the Si substrate.

On the other hand, for both the SiC and Si substrates, the peak frequency of the TO mode of the oxide is red-shifted toward the interface of the oxide and substrate. There are several possible explanations for the band shift: The dependence of the peak frequency of the TO mode on the strain or substoichiometry in the oxide; roughness at the interface between the oxide and the substrate; and optical phenomena including image charge effects and electromagnetic phase shifts.[14] Several previous papers[10,11] reported that the peak frequency of the TO mode is usually red-shifted as the oxide thickness decreases; this is consistent with our Si data shown in Fig. 5-4(b). However, the degree of the shift of the TO mode for the oxide on the SiC substrate is smaller than that for the oxide on the Si substrate toward the interface of the oxide and substrate. In case of the oxide on the SiC substrate, the net TO peak-shift is the result of competition between the red shift at the oxide/SiC interface and the blue shift by compressive stress. Thus, it is difficult to compare the degree of the red shift on the Si and SiC substrates.

Figures 5-7(a) and (b) show the depth profiles of carbon and nitrogen, respectively,

measured by SIMS. The amount of carbon impurity in the oxide for sample OX is larger than that for samples NO and NL, which are under the detection limit. We assume that the POA treatment in a NO atmosphere has the effect of removing the carbon impurities from the oxide, which is consistent with the result reported for N_2O oxidation.[7] The nitrogen impurity levels rise sharply at the oxide/SiC interface for samples NO and NL. The amount of nitrogen in sample NL that received POA for a longer time is slightly larger than that in sample NO at the oxide/SiC interface. When the amount of nitrogen becomes too large at the oxide/SiC interface, the density of fast interface states increases significantly and the channel mobility starts to drop.[40] The aggregated nitrogen at the interface might play a crucial role in achieving high channel mobility.

To clarify the origin of the red shift of the TO mode at the oxide/SiC interface, we measured CL spectra of the non-etched thermal oxides, at acceleration voltages of 3 kV and 5 kV as shown in Fig. 5-8(a) and (b). We used different acceleration voltages to distinguish between defects in the oxide (3 kV) and defects near the interface (5 kV). CL peaks are observed at 450, 485, 660, and 900 nm for the oxides on the 4H-SiC substrates. The peak and dip in Fig. 8 at ~900 nm may be caused by unknown defects, or they may be caused by a combination of the overtone of the CL peak at ~500 nm with absorption in the optical fiber. The CL peaks at 460 and 490 nm are attributed to oxygen vacancy centers (OVCs), whereas the CL peak at 660 nm is attributed to non-bridging oxidation hole centers (NBOHCs).[11–13] As shown in Fig. 5-8(b), broad luminescence near 560 nm appears for samples NO and NL, which were given a post-annealing treatment in a NO ambient. This peak originates from defects related to Si–N bonds as previously reported[41] and overlaps with the peaks caused by the OVCs. Thus, The CL intensity from OVCs for samples NO and NL decreases compared with that of sample OX. It is very likely that the number of defects for sample OX is larger than those for samples NO and NL. Thus, the compressive stress at the oxide/SiC interface

generates Si suboxides and weakens the Si-O bonds. As the result, the oxygen deficiency increases in order to relax the compressive stress in the oxide with a thickness less than 3 nm.

CONCLUSION

We measured the FT-IR spectra of thermal oxides with different electrical properties and various thicknesses grown on 4H-SiC substrates. The peak frequency of the TO mode is blue-shifted as the thickness of the oxide layer decreases down to 3 nm. The blue shift of the TO mode indicates the existence of interfacial compressive stress in the oxide. The blue shift of sample OX is larger than that of samples NO and NL for thick oxide with a thickness of 3–8 nm. The compressive stress for sample OX is larger than that of sample NO and NL.

Comparing the data for the oxide on a SiC substrate with that for similar oxide on a Si substrate, we have concluded that the interfacial stress for the oxide on the SiC substrate is larger than for that on the Si substrate. The difference of peak shifts between Si and SiC substrates is caused by different thermal expansions and elastic moduli between the SiC and Si substrates.

For the thinner thermal oxides (SiO_2 thickness less than 3 nm), the peak frequency of the TO mode of the oxides on the 4H-SiC substrate is red-shifted as the oxide layer thickness decreases. The TO mode peak-frequency shift for the sample that did not have post-oxidation annealing (sample OX) is larger than that for the samples that had been subjected to a post-oxidation annealing in nitric oxide (samples NO and NL). The channel mobilities are correlated with the degree of the shift of the TO mode in samples with an oxide thickness of less than 3 nm. These results indicate that the chemical structure of sample OX changes drastically near the oxide/Si interface region within 3 nm from the SiC surface compared with that of samples NO and NL.

The SIMS results show that the nitrogen impurity levels rise sharply at the oxide/SiC interface for samples NO and NL. The aggregated nitrogen at the interface might play a crucial role in achieving high channel mobility.

The amount of OVCs for sample OX is larger than that of sample NO and NL, as determined by CL measurements. The compressive stress at the oxide/SiC interface generates silicon suboxide components and weakens the Si-O bonds. As the result, the oxygen deficiency increases in order to relax the compressive stress in the oxide less than 3 nm thickness.

In this way, the FT-IR study has provided us with novel and unique information about the stress and inhomogeneity at the oxide /SiC interface.

REFERENCES

[1]K. Fukuda, M. Kato, K. Kojima, J. Senzaki. Appl. Phys. Lett. 84(12), 2088(2004).

[2]S. Dimitrijev, H.F. Li, H.B. Harrison, D. Sweatman. IEEE Trans. Electron Dev. Lett. 18(5), 175 (1997).

[3]G.Y. Chung, C.C. Tin, J.R. Williams, K. McDonald, R.K. Chanana, R.A. Weller, S.T. Pantelides, L.C. Feldman, O.W. Holland, M.K. Das, J.W. Palmour. IEEE Electron Device Lett. 22(4), 176(2001).

[4]C.-Y. Lu, J.A. Cooper Jr., T. Tsuji, G. Chung, J.R. Williams, K. McDonald, L.C. Feldman. IEEE Trans. Electron Devices 2003. 50(7), 1582 (2003).

[5]S. Dhar, S. Wang, J.R. Williams, S.T. Pantelides, L.C. Feldman. Mater. Res. Soc. Bull. 30(4), 288 (2005).

[6]L.A. Lipkin, M.K. Das, J.W. Palmour. Mater. Sci. Forum 2002. 389-393, 985 (2002).

[7]T. Kimoto, Y. Kanzaki, M. Noborio, H. Kawano, H. Matsunami. Jpn. J. Appl. Phys. 44(3R), 1213 (2005).

[8]D. Okamoto, H. Yano, T. Hatayama, T. Fuyuki. Appl. Phys. Lett. 96(20), 3508 (2010).

[9]N.J. Harrick. Internal Reflection Spectroscopy. 2nd ed. New York: Wiley-Interscience, 1967. p. 51.

[10]C. Martinet, R.A.B. Devine. J. Appl. Phys. 77(9), 4343 (1995).

[11]K.T. Queeney, M.K. Weldon, J.P. Chang, Y.J. Chabal, A.B. Gurevich, J. Sapjeta, R.L. Opila. J. Appl. Phys. 87(3), 1322(2000).

[12]N. Nagai, K. Terada, Y. Muraji, H. Hashimoto, T. Maeda, Y. Maeda, E. Tahara, N. Tokai, and A. Hatta, J. Appl. Phys. 91, 4747 (2002).

[13]K. Kim, J. Song, D. Kwon, G.S. Lee. Appl. Phys. Lett. 72, 1247 (1998).

[14]I. Boyd, J. Wilson. Appl. Phys. Lett. 50(6), 320 (1987).

[15]M.L. Green, E.P. Gusev, R. Degraeve, E.L. Garfunkel. J. Appl. Phys. 90(5), 2057 (2001).

[16]N. Hirashita, S. Tokitoh, H Uchida. Jpn. J. Appl. Phys. 32(4R), 1787 (1993).

[17]J. Shiuh, Si-chen Lee. J. Appl. Phys. 77(4), 1805 (1995).

[18]T. Yamaguchi, N. Sakamoto. J. Appl. Phys. 83, 554 (1998).

[19]Y. Kim, M. Hwang, H. Kim. J. Appl. Phys. 90(7), 3367 (2001).

[20]R. Nonogaki, S. Nakai, S. Yamada, T. Wada. J. Vac. Sci. Technol. A. 16(5), 2827 (1998).

[21]P.G. Pai, S.S. Chao, Y. Takagi, G. Locovsky. J. Vac. Sci. Technol. A. 4(3), 689 (1986).

[22]J.T. Fitch, G. Lucovsky, E. Kobeda, E.A. Irene. J. Vac. Sci. Technol. B. 7(2), 153 (1989).

[23]G. Lucovsky, M.J. Manitini, J.K. Srivastava, E.A. Irena. J. Vac. Sci. Technol. B. 5(2), 530 (1987).

[24]W.A. Pliskin, H.S. Lehman. J. Electrochem. Soc. 112(10), 1013 (1965).

[25]S. Miyazaki, H. Nishimura, M. Fukuda, L. Ley, J. Ristein. Appl. Surf. Sci. 113/114, 585 (1997).

[26]R.A.B. Devine. Appl. Phys. Lett. 68(22), 3108 (1996).

[27]J.-S. Chou, S.-C. Lee. J. Appl. Phys. 77(4), 1805 (1995).

[28]H. Hirai, K. Kita. Appl. Phys. Lett. 103(13), 132106 (2013).

[29]M. Yoshikawa, H. Seki, K. Inoue, K. Matsuda, Y. Tanahashi, H. Sako, Y. Nanen, M. Kato, T. Kimoto. Appl. Spectrosc. 65(5), 543 (2011).

[30]M. Yoshikawa, H. Seki, T. Yamane, Y. Nanen, M. Kato, T. Kimoto. Appl. Spectrosc. 67(5), 542 (2013).

[31]M. Yoshikawa, H. Seki, K. Inoue, Y. Nanen, T. Kimoto. Appl. Spectrosc. 68(10), 1176 (2014).

[32]H. Hashimoto, Y. Hijikata, H. Yaguchi, S. Yoshida. Appl. Surf. Sci. 255(20), 8648 (2009).

[33]T. Hosoi, T. Kirino, S. Mitani, Y. Nakano, T, Nakamura, T. Shimura, H. Watanabe. Current. Appl. Phys. 12(3), S79 (2012).

[34]E. Pippel, J. Woltersdorf, H. Ólafsson, E. Sveinbjörnsson. J. Appl. Phys. 97, 034302 (2005).

[35]J. Taillon, J. Yang, C. Ahyi, J.Rozen, J. William, L. Feldman, T. Zheleva, A. Lelis, L.

Salamanca-Riba. J. Appl. Phys. 113, 044517 (2013).

[36]M. Yoshikawa, K. Matsuda, Y. Yamaguchi, T. Matsunobe, Y. Nagasawa, H. Fujino, T. Yamane. J. Appl. Phys. 92(12), 7153 (2002).

[37]M. Yoshikawa, S. Ogawa, K. Inoue, H. Seki, Y. Tanahashi, H. Sako, Y. Nanen, M. Kato, T. Kimoto. Appl. Phys. Lett. 100(8), 082105 (2012).

[38]M. Yoshikawa, H. Seki, K. Inoue, T. Kobayashi, T. Kimoto, Mater. Sci. Forum 2015. 821-823, 460 (2015).

[39]K. Chokawa, S. Kato, K. Kamiya1, K. Shiraishi. Mater. Sci. Forum 2013. 740–742,469 (2013).

[40]H. Yoshioka, T. Nakamura, T. Kimoto. J. Appl. Phys. 111(2), 024520 (2012).

Table 5-I. Original thickness, oxidation conditions, and channel mobility of the 4H-SiC (0001) MOS structures investigated in this study.

Sample No.	Original thickness(nm)	Thermal oxidation	Post-oxidation	Mobility (cm^2/Vs)
OX	75	1300℃ 60 min	—	5～8
NO	76	1300℃ 60 min	NO anneal 1250℃ 30 min	35～38
NL	76	1300℃ 60 min	NO anneal 1250℃ 180 min	30～34

*) The channel mobility was obtained for 4H-SiC(0001) MOSFETs fabricated on p-type epilayers with an acceptor concentration of about 1×10^{16} cm^{-3}.

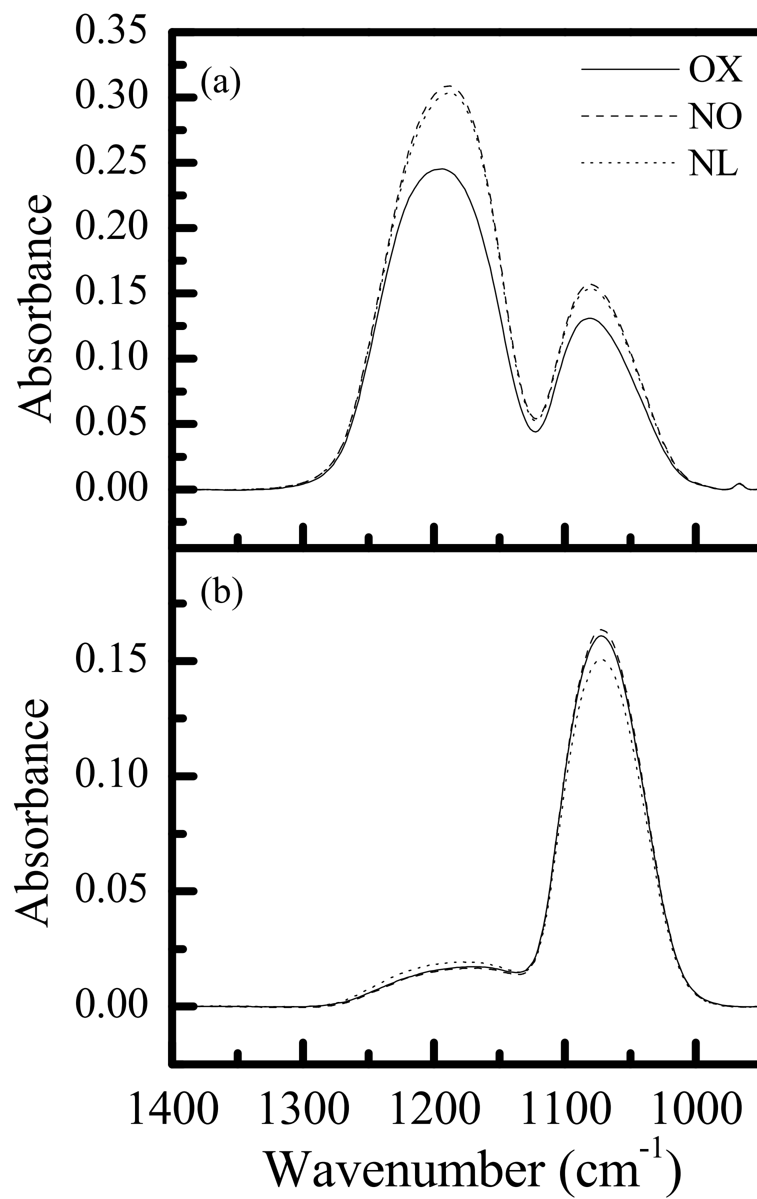

Fig. 5-1. ATR spectra of the non-etched oxides measured using (a) p- and (b) s-polarized IR light.

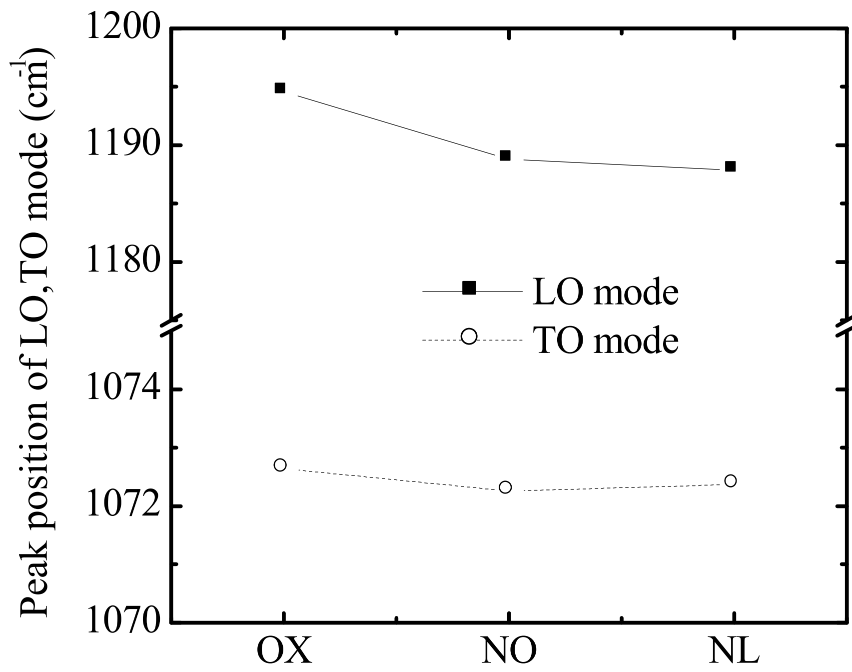

Fig. 5-2. Peak positions of the LO and TO modes for non-etched oxides. The oxide thicknesses are shown in Table I.

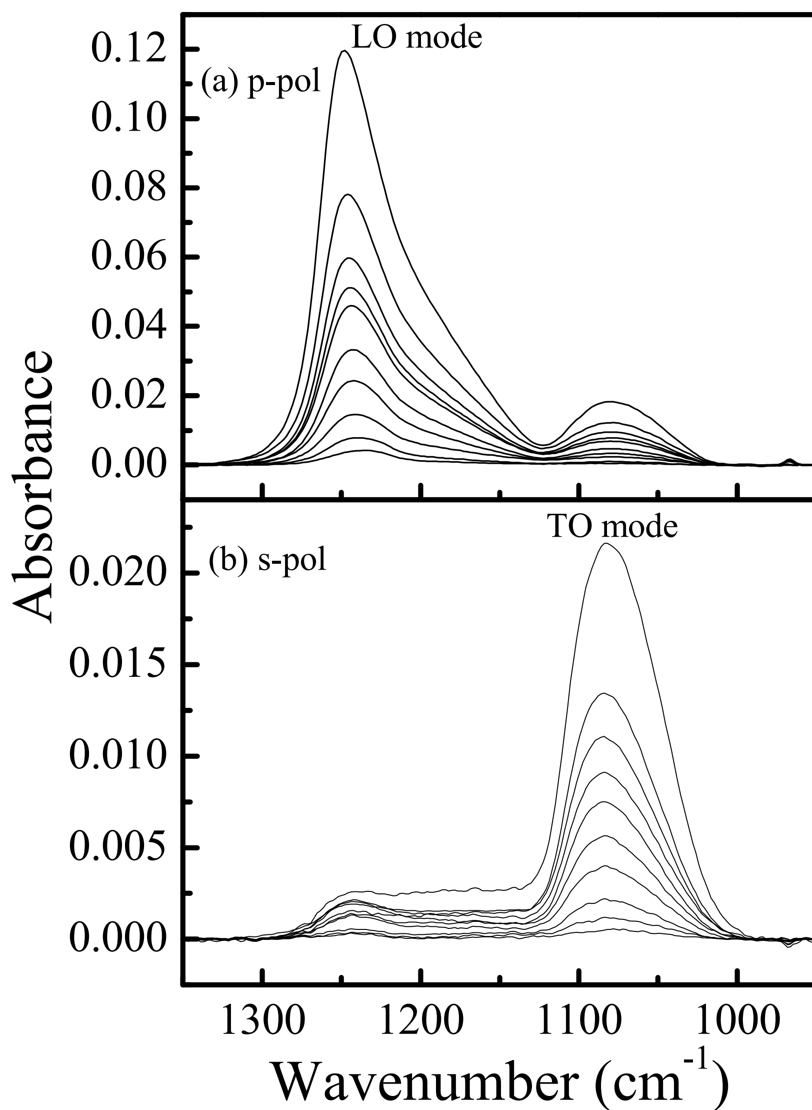

Fig.5-3. ATR spectra of sample OX measured using (a) p-polarized and (b) s-polarized IR light for various SiO_2 thicknesses ranging from 8 to 0 nm in steps of about 0.8 nm prepared by wet etching in 1% hydrofluoric acid solution.

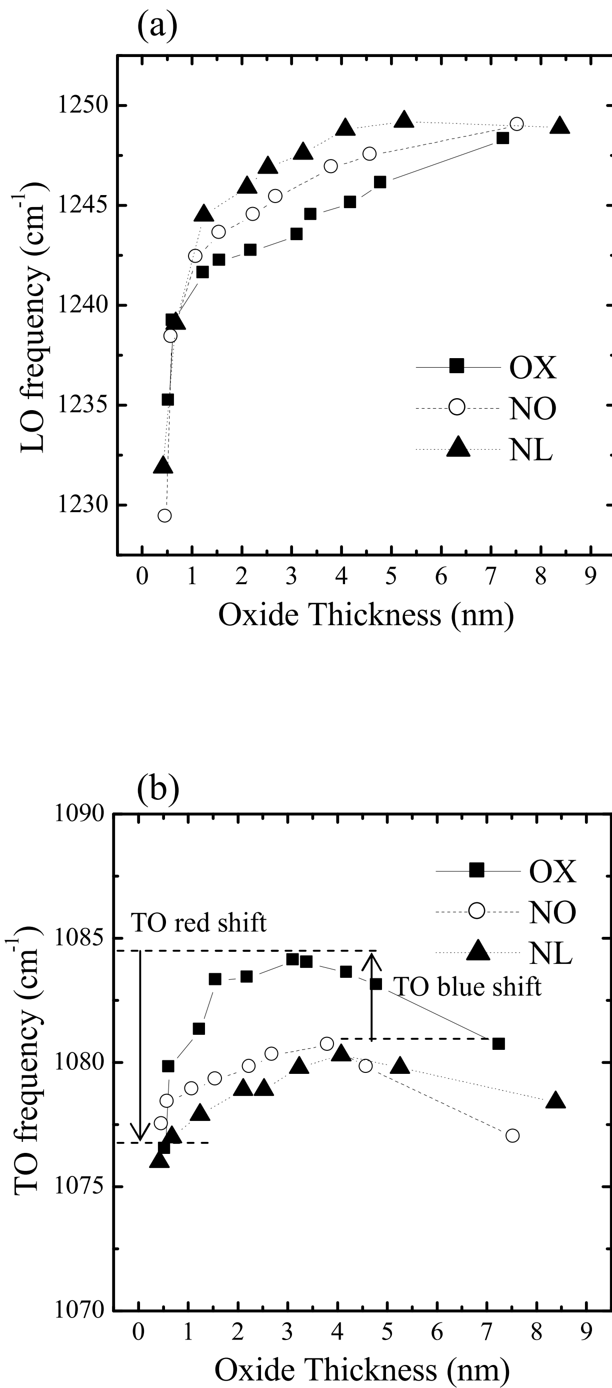

Fig. 5-4. Thickness dependence of the LO and TO mode peak frequencies measured by polarized infrared light. (a) LO frequency measured by p-polarized light as a function of oxide thickness (b) TO frequency measured by s-polarized light as a function of oxide thickness.

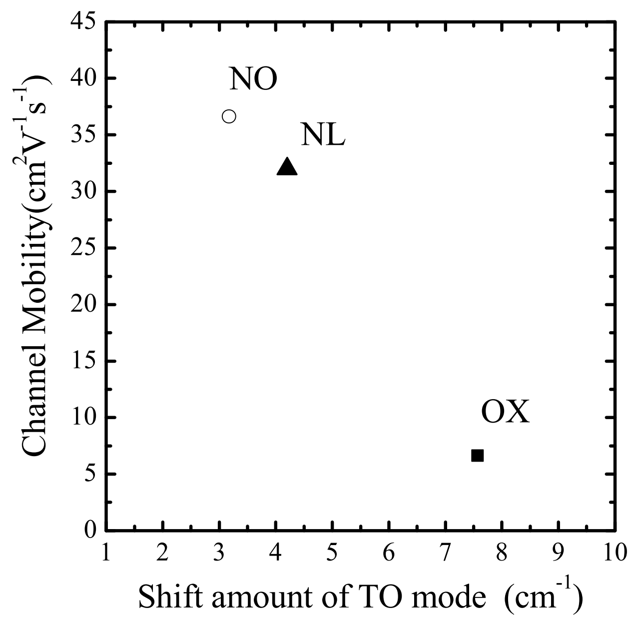

Fig. 5-5. Red shift of the TO mode of an oxide with a thickness of less than 3 nm vs. channel mobility.

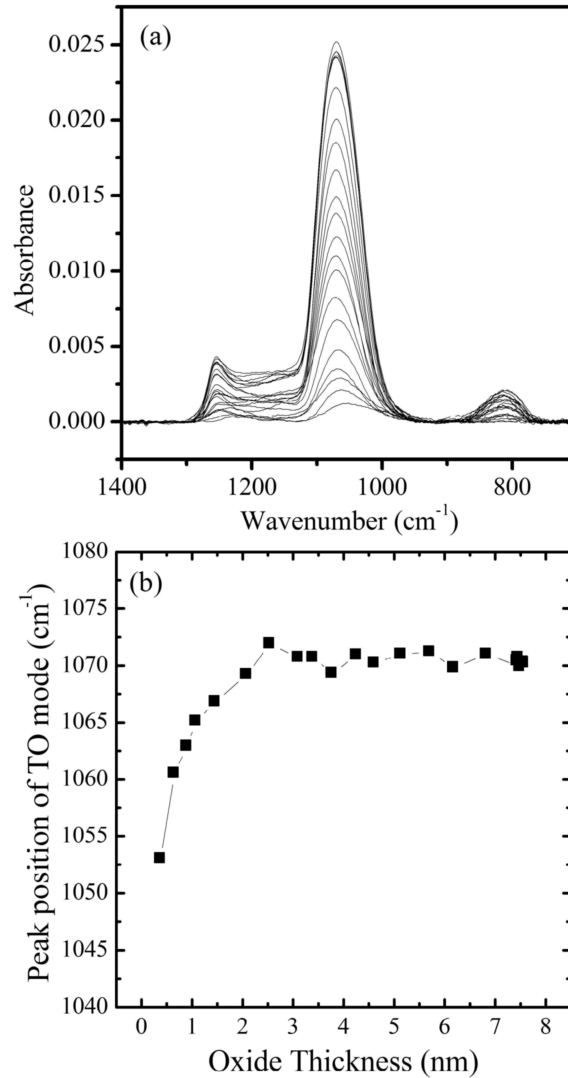

Fig. 5-6. Infrared absorption data of the thermal oxide on a silicon substrate. (a)Transmittance spectra of thermal oxide on a silicon substrate for various SiO_2 thicknesses that had been decreased from 8 nm to 0 nm by wet etching in 1% hydrofluoric acid solution. (b) Thickness dependence of the TO mode peak frequency measured by transmittance measurements.

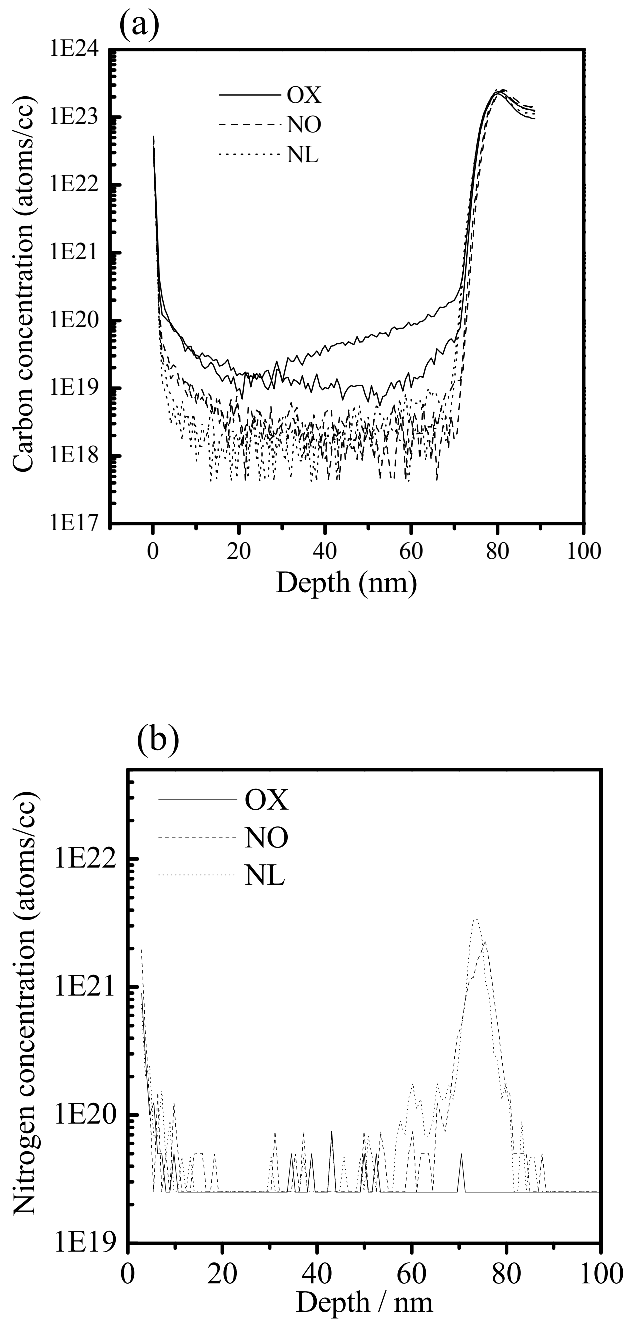

Fig. 5-7. Depth profiles of impurities measured by secondary ion mass spectroscopy. (a) Depth profiles of the amount of carbon impurity in the oxides. (b) Depth profiles of the amount of nitrogen impurity in the oxides.

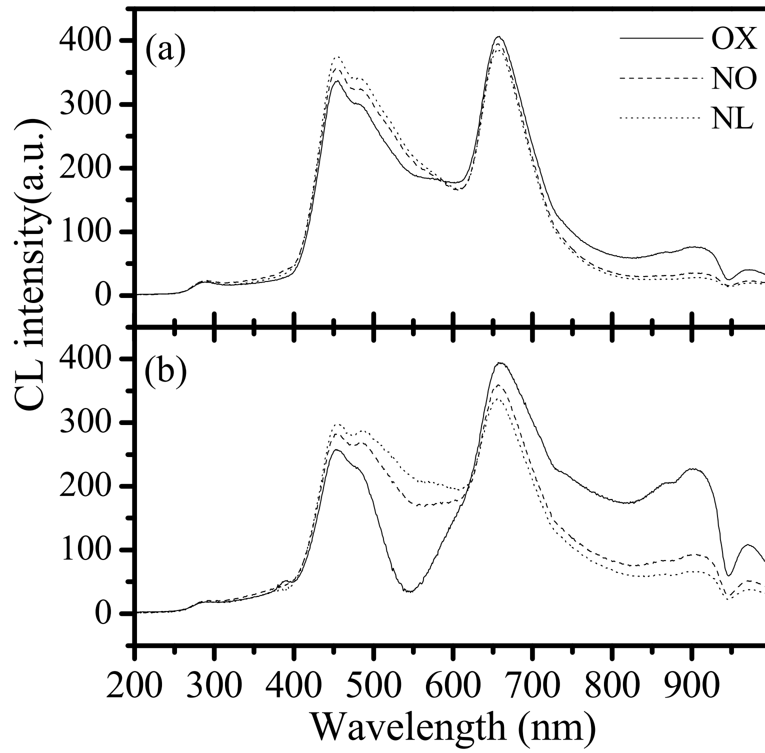

Fig. 5-8. Cathode luminescence (CL) spectra of the samples measured at acceleration voltages of (a) 3 kV and (b) 5 kV. The spectra shown here were obtained by subtracting the CL spectrum of the 4H-SiC substrate.

List of Research Publications

Original papers:

1. H. Seki, K. Inoue, N. Nagai, M. Shimada, K. Inukai, S. Ogawa: Characterization of ashing damage in depth in Low-k dielectric films by micro beam IR method, Proc. AMC 2004, pp. 375-380.
2. H. Seki, H. Hashimoto, and Y. Ozaki: Characterization of process-induced damage in Cu/low-k interconnect structure by microscopic infrared spectroscopy with polarized infrared light, J. Appl. Phys. 120(9), (2016) 095301-95306.
3. M. Yoshikawa, H. Seki, K. Inoue, Y. Nanen, and T. Kimoto: Characterization of Inhomogeneity in Silicon Dioxide Films on 4H-Silicon Carbide Epitaxial Substrate Using a Combination of Fourier-Transform Infrared and Cathodoluminescence Spectroscopy, Appl. Spectrosc, 68(10), (2014)1176-1180.
4. H. Seki, M. Yoshikawa, T. Kobayashi, T. Kimoto, and Y. Ozaki: Characterization of Thermal Oxides on 4H-SiC Epitaxial Substrates Using Fourier-Transform Infrared Spectroscopy, Appl. Spectrosc, in press.

Associated papers:

5. H. Seki, M. Takada, T. Tanabe, T. Wadayama, A. Hatta: Infrared absorption study of CO chemisorption on copper island films, Surface Science, 506(2002)23-32.
6. Y. Suzuki, H. Seki, T. Inamura, T. Tanabe, T. Wadayama, A. Hatta: Enhancement of the infrared absorption of methanol adsorbed on silver island films, Surface Science, 433-435 (1999) 261-266.
7. Y. Suzuki, H. Seki, T. Inamura, T. Tanabe, T. Wadayama, A. Hatta: Enhancement of the infrared absorption of methanol adsorbed on silver island films, Surface Science, 433-435 (1999) 261-266.
8. M.Yoshikawa, H. Seki, K. Inoue, K. Matsuda, Y. Tanahashi, H. Sako, Y. Nanen, M. Kato, and T. Kimoto: Characterization of silicon dioxide films on a 4H-SiC Si(0001) face by fourier transform infrared (FT-IR) spectroscopy and cathodoluminescence spectroscopy. Appl. Spectrosc, 65 (2011) 543-548.
9. M.Yoshikawa, H. Seki, T. Yamane,Y. Nanen, M. Kato, and T. Kimoto: Abnormal Behavior of LO phonon in Silicon Dioxide Films on 4H-SiC Bulk Epitaxial Substrate by Fourier Transform Infrared (FT-IR) Spectroscopy, Appl. Spectrosc, 67(2013) 542-545.
10. M.Yoshikawa, H. Seki, K. Inoue, T. Kobayashi, T. Kimoto: Characterization of Thermal Oxides on 4H Silicon Carbide (4H-SiC) Epitaxial Substrate Using Fourier Transform Infrared Spectroscopy, Appl.Spectrosc, (2015), in press.
11. M.Yoshikawa, S. Ogawa, K. Inoue, H. Seki, H. Sako, Y. Nanen, M. Kato, and T. Kimoto: Characterization of silicon dioxide films on 4H-SiC Si (0001) face by

cathodoluminescence spectroscopy and x-ray photoelectron spectroscopy, Applied Physics Letters, 100 (2012), 082105.

12. M.Yoshikawa, K. Inoue, H. Seki, Y. Nanen, M. Kato, and T. Kimoto: Characterization of silicon dioxide films on 4H-SiC (0001) Si, (1-100) M, and (11-20) A faces by cathodoluminescence spectroscopy, Applied Physics Letters, 102 (2016), 051612.
13. S. Ogawa, H. Seki, Y. Otsuka, S. Nakao, Y. Takigawa, H. Hashimoto: Micro Beam IR Characterization of Narrow Width (-100 nm) Low-k Spaces Between Cu Lines Correlated with Valence EELS Evaluation, Proc. IITC 2009, pp.76.
14. H. Seki, N. Tarumi, Y. Shimizu, Y. Otsuka, H. Hashimoto, S. Ogawa: Characterization of damage of Low-k films between Narrow Cu lines by micro beam IR method, Proc. AMC 2009, pp. 647.
15. M. Takeda, N. Matoba, K. Matsuda, H. Seki, K. Inoue, M. Oishi, M. Sakai: Effect of ultraviolet cure on the interfacial toughness and structure of SiOC thin film on Si substrate, Journal of Materials Research, 25 (2010) 1910-1916.
16. R. Sugie, K. Kosaka, H. Seki, H. Hashimoto, M. Yoshikawa: Measurement of temperature-dependent stress in copper-filled silicon vias using polarized Raman spectroscopy, J. Appl. Phys. 114 (2013) 233503.
17. N. Man, H. Okumura, H. Oizumi, N. Nagai, H. Seki, I. Nishiyama: Depth profile analysis of chemically amplified resist by using TOF-SIMS with gradient shaving preparations, Appl. Surf. Sci, 231-232 (2004) 353-356.
18. N. Nagai, T. Imai, K. Terada, H. Seki, H. Okumura, H. Fujino, T. Yamamoto, I. Nishiyama, A. Hatta: Depth profile analysis of ion-implanted photoresist by infrared spectroscopy, Surface and Interface Analysis (2002) 545 – 551.
19. S. Yamamoto, D. Kitazawa, J. Tsukamoto, T. Shibamori, H. Seki, Y. Nakagawa: Composition depth profile analysis of bulk heterojunction layer by time-of-flight secondary ion mass spectrometry with gradient shaving preparation, Thin Solid Films, 518 (2010) 2115–2118.
20. F. Inoue, T. Shimizu, H. Miyake, R. Arima, T. Ito, H. Seki, Y. Shinozaki, T. Yamamoto, S. Shingubara: Adsorption of Pd nanoparticles catalyst in high aspect ratio through-Si vias for electroless deposition, Electrochimica Acta, 82 (2012) 372-377.
21. N. Inoue, Y. Goto, H. Seki, K. Watanabe, H. Oyama, Y. Kawamura: Infrared measurement and irradiation of ultra low carbon concentration silicon crystal, Physica Status Solidi (c), 9 (2012) 1931–1936.
22. N.Inoue, Y.Goto, T.Sugiyama, H.Seki, K.Watanabe, Y.Kawamura: Infrared Defect Dynamics of Irradiation Induced Complexes in CZ Silicon - C-Rich Case, Solid State Phenomena. 205-206, (2013) 228-232.

Book chapters:

1. S. Ochiai and H. Seki: Chapter 16 “Infrared Microspectroscopic Measurements” ; Editor. M. Tasumi : Introduction to Experimental Infrared Spectroscopy, John Wiley & Sons, 223-240 (2015).

ACKNOWLEDGEMENTS

The author expresses his sincere gratitude to his supervisor, Professor Yukihiro Ozaki, Kwansei Gakuin University, for providing this valuable study opportunity.

The author especially expresses his deepest appreciation to his supervisors at Toray Research Center, Inc., Dr. Masanobu Yoshikawa and Mr. Hideki Hashimoto, for their guidance, considerable encouragement, and invaluable discussions that propelled this research.

The author is very grateful to Professor Tsunenobu Kimoto (Kyoto University), Dr. Shinichi Ogawa (NIMS), Dr. Miyoko Shimada (Toshiba), Dr. Yuji Otsuka, Dr. Keiko Matsuda, Ms. Yumiko Shimizu, Ms. Keiko Inoue and Ms. Chie Sugishita, of Toray Research Center, Inc., for their valuable cooperation with the experiments.

The author is also grateful to the members of the Materials Science Laboratory of Toray Research Center, Inc. for their encouragement, suggestions, and comments.

Finally, the author would like to extend his indebtedness to his family for their understanding, support, encouragement, and sacrifices throughout the course of this study.